Desalination and Water Treatment
www.deswater.com
doi: 10.5004/dwt.2023.30200

316 (2023) 335–355
December

Oil removal from water using agricultural wastes-based adsorbents for the application in reverse osmosis desalination systems

Nora Wagih*, Mohamed M. Mahmoud, Amro A. Elbaz, Diaa EL-Moniry

Environmental Engineering Department, Faculty of Engineering, Zagazig University, Zagazig 44519, Egypt, emails: nora.wagih@yahoo.com (N. Wagih), mbasuny@zu.edu.eg (M.M. Mahmoud), elbaz50@hotmail.com (A.A. Elbaz), dsmonayeri@yahoo.com (D. EL-Moniry)

Received 1 September 2023; Accepted 3 December 2023

ABSTRACT

Egypt is facing water shortage due to limitation in the freshwater resources and the increased population growth. Thus, there is a need for developing new water resources such as the expansion in building large-scale reverse osmosis (RO) seawater desalination plants. Oil spill in the marine environment can cause severe fouling problems and make damage to the RO membranes, which increases the operating cost. The current study focuses on oil removal from water using agricultural-based adsorbents to reduce the membrane fouling in the RO systems. Three adsorbents namely: rice husk (RH), sawdust (SD) and sugarcane bagasse (SCB) were tested to remove used motor oil (UMO) and crude oil (CO) from distilled and raw seawater. Activated carbon (AC) was included in the measurements to be used as a reference case to compare with. The oil sorption removal and adsorption capacity were determined experimentally for the four tested adsorbents. The experimental parameters included: initial oil concentration (2–40 g/L), adsorbent dose (2–30 g/L), contact time (5–120 min), agitation time (0–60 min), chemical modification (acid vs. base treatment), water salinity (up to 35 g/L). The effect of the presence of other heavy metals on oil sorption removal and adsorption capacity was also investigated. The characteristics of the adsorbents surface were studied using the Fourier-transform infrared spectroscopy, scanning electron microscopy, and Brunauer–Emmett–Teller analysis. The results demonstrated that the adsorption removal of UMO with higher viscosity is higher than CO and always the RH exhibited the highest adsorption capacity compared to SD and SCB but about 30% less than AC. Precaution should be taken when distilled water is used rather than raw seawater because the difference could reach about 50% but it depends on the type of oil and adsorbing material. Additionally, the oil sorption removal in seawater is about 20% higher in raw seawater compared to distilled water. The oil sorption removal increased with an increase in contact time, adsorbent dosage, agitation time, and salinity, and decrease in initial oil concentration. The effect of presence of metals ions concentration in raw seawater can be neglected with the adsorbent used in the current study. The adsorption isotherm models by Langmuir described the experimental data very well while the pseudo-second-order described the kinetics data very well. The small difference in performance between RH and AC indicates that RH is very promising low-cost adsorbents for oil removal in RO desalination systems. The Gibbs free energy (ΔG) was calculated and the values were negative, indicating that the sorption process was spontaneous.

Keywords: Reverse osmosis desalination; Adsorption; Agricultural waste; Seawater; Oil removal; Isotherm kinetics

* Corresponding author.

1. Introduction

It is well-known that Egypt is an arid area with low rainfall and most of the freshwater comes through the Nile River at a rate of 55.5 billion·m^3/y, which is a fixed share according to the 1959 agreement between Egypt and Sudan. Additionally, the Nile River accounts for the large majority of all water demand in Egypt. The problem is that the quantity of water supplied by the Nile River is significantly affected by many factors such as climate changes and political conflict among the Nile basin countries. In other words, the Egyptian water resources are limited and are very challenging. Abd Ellah [1] summarized the challenges facing Egypt as follows: (i) the increased water demand due to the rapid population growth, industrialization and sustainable development plans, (ii) the conflict among the Nile basin countries, for example, the Grand Ethiopian Renaissance Dam is expected to reduce the water flow through the Nile River, (iii) the climate changes could affect the Nile River basin through draught or flooding, (iv) the scarcity of other water resources such as rainfall, (v) the environmental restrictions on the reuse of drainage water, and (vi) the high cost of desalination plants. Accordingly, effective and economic strategies are needed to overcome the water shortage in Egypt, which is also a global problem. For example, Janowitz et al. [2] reported that the Middle East will face severe water shortage by 2050, which can be mitigated by the construction of large-scale reverse osmosis (RO) seawater desalination plants.

Reverse osmosis (RO) is one of the most widely used technologies in seawater and brackish water desalination. However, its operation is significantly affected by many factors, among which is the membrane fouling. Jiang et al. [3] and AlSawaftah et al. [4] reported that membrane fouling can lead to the following issues: (i) performance degradation, (ii) short operating period, (iii) low permeate flux, (iv) low solute removal efficiency, (v) short membrane lifetime, and (vi) higher operating pressure. Additionally, fouling can increase the operating cost of RO plants. For example, Jafari et al. [5] conducted an economic evaluation study to estimate the cost of membrane fouling in seven large-scale desalination plants in the Netherland. The evaluated plants included four nano-filtration plants and three RO plants. The fouling cost was estimated in terms of the energy cost induced by the increased feed pressure, cost of reduction in water permeability, cost of early membrane replacement and cost of extensive in-place cleaning. It was found that the average cost of fouling is 11% of the operating cost in the nano-filtration plants while it was 24% in the RO systems. It is worth mentioning that the feed water in the evaluated plants was groundwater and water from the river, which have low salinity compared to the seawater. In other words, the fouling cost is expected to be larger in case of seawater desalination plants. It may be concluded that reducing the fouling problem could help reduce the operating cost in RO plants.

Membrane fouling can be reduced either by selecting an effective pre-treatment method or developing novel materials for the fabrication of the RO membranes. The selection of the pre-treatment method may depend on the type of foulants which include colloids, organic, inorganic, and biological foulants. The organic foulants exist in many forms such as fats, greases, oils, carbohydrates, and bio-colloids as reported by Qasim et al. [6] and Yiantsios et al. [7]. Among organic foulants, oils may represent the large component, especially in the oceans and seawater, due to the accidents of oil spillage during oil explorations and transportation, as cited by Sarkheil and Tavakoli [8]. The problem with oil pollution is that the chemical/physical properties of the spilled oil change dramatically due to weathering processes (evaporation, dissolution, dispersion, photochemical oxidation, microbial degradation and adsorption on suspended materials, agglomeration), which enhance its dissolution in the seawater (emulsified oil) and consequently make its removal more complicated as cited by Jian et al. [9]. In other words, it may be difficult to remove the emulsified oil from seawater using the conventional techniques such as oil floatation and skimming. Jian et al. [9] studied oil removal from contaminated seawater using various pre-treatment methods (advanced oxidation, ultrafiltration, coagulation and adsorption by granular activated carbon, biological treatment and low-pressure RO membrane). The contaminated seawater was simulated using weathered oil, that is, the oil was mixed with the seawater and left in the atmosphere exposed to photooxidation and microbial degradation for one month. It is worth mentioning that during the weathering process, the initially insoluble oil is converted into soluble compounds with relatively low molecular weight. It was concluded that adsorption using granular activated carbon was the most efficient process compared to the other tested methods. Accordingly, the current study focuses on oil removal by adsorption motivated by its simplicity and the possibility to use low-cost adsorbents such as agricultural wastes, which may help to reduce the pre-treatment cost in the RO desalination plants. In literature, there are many adsorbents tested by researchers for oil removal from wastewater or synthetic seawater as will be discussed in the following paragraphs.

A group of researchers tested corn wastes as adsorbing materials for oil removal from synthetic seawater. Asadpour et al. [10] studied the effect of oil viscosity (by testing two different types of oils) on the adsorption capacity of corn silk. It was found that the untreated (raw) corn silk achieved maximum adsorption capacity of 8,150 and 9,400 mg·oil/g adsorbent for the high and low viscosity oil, respectively while the chemically treated corn silk achieved 14,020 and 16,680 mg·oil/g adsorbent for the high and low viscosity oil, respectively. In other words, the adsorption capacity has increased significantly with the treated corn silk and increased slightly with decreasing the oil viscosity. Zhen et al. [11] studied the effect of initial oil concentration (40–200 mg/L) and pH on the adsorption capacity of chemically treated and untreated corn cobs. In their experiments, crude oil was mixed with deionized water and was emulsified by a surfactant. The results demonstrated that the adsorption capacity increased as the initial oil concentration increased, which was attributed to the increased chance of oil collision with the adsorbent surface while it decreased as the pH increased. The treated corn cobs achieved maximum adsorption capacity of 16,520 mg·oil/g adsorbent at pH = 5 while the raw corn cobs achieved 6,860 mg·oil/g adsorbent. In other words, the treatment method adopted in

their study enhanced the adsorption capacity by 141%. Peng et al. [12] modified the corn stalk and corncobs biologically by a kind of fungi for oil removal from oil/water mixture (oil mixed with deionized water at a concentration of 133 g/L). It was found that the adsorption capacity increased from 6,950 mg·oil/g adsorbent for raw corn stalk to 9,030 mg·oil/g adsorbent for treated corn stalk or about 30% enhancement while for the corncobs, it increased from 4,140 mg·oil/g adsorbent (raw) to 7,690 mg·oil/g adsorbent (modified) or about 86% enhancement. Choi [13] studied the use of raw corncobs and pulverized corncobs for crude oil removal from water (oil was added to deionized water) with oil concentration in the range 200–1,500 mg/L and adsorbent dosage 0.5–5 g. It was found that the adsorption capacity increased with increasing the adsorbent dosage and was attributed to the increase in surface area and the number of active sites. The maximum adsorption capacity reached 7,800 mg·oil/g adsorbent and 4,210 mg·oil/g adsorbent for the pulverized corncobs and raw corncobs, respectively (85% enhancement due to pulverization). It may be concluded from the above studies that, among the tested corn by-products, the treated corn silk achieved the highest adsorption capacity (16,680 mg/g) with a low viscosity oil.

Another group of researchers tested treated and untreated bagasse to be used as an adsorbing material for oil removal. Sarkheil and Tavakoli [8] used chemically treated nano-size bagasse for the removal of an emulsified oil (using surfactant) from water with initial oil concentration in the range 200–1,000 ppm. Their results indicated that the oil removal efficiency decreased from about 60% to about 30% with the increase in the initial oil concentration. On the contrary, it increased from about 40% to about 60% when the adsorbent dose was increased from 2 to 10 g at a fixed oil concentration of 600 ppm. Abdelwahab et al. [14] used raw and chemically-treated bagasse for oil removal from artificial seawater at a wide range of pH values. The treated bagasse was coated with a hydrophobic polymer. Four types of oil were tested namely; diesel oil, paraffin oil, gasoline oil and vegetable oil. It was found that the pH value does not affect the adsorption capacity while the maximum adsorption capacity was found to depend on the type of oil, especially for the treated bagasse while the effect was insignificant for the raw bagasse. The highest adsorption capacity was achieved with the polymer-coated bagasse where it reached 8,400 mg·oil/g adsorbent (236% enhancement) for diesel oil, 11,600 mg·oil/g adsorbent (329.6% enhancement) for paraffin oil, 7,600 mg·oil/g adsorbent (230% enhancement) for gasoline oil and 10,700 mg·oil/g adsorbent (311% enhancement) for vegetable oil. Abdelwahab et al. [15] studied the use of raw bagasse, surfactant modified bagasse and a mixture of polystyrene foam and surfactant modified bagasse as adsorbents for the removal of emulsified oil (food oil) from water at different pH values. It was found that, for the mixture, the oil adsorption capacity and removal efficiency depend on the mixing ratio. They increased as the mixing ratio (by mass) was increased from 0.5 to 1 while the effect was insignificant for mixing ratios greater than 1. Additionally, the adsorption capacity was found to increase gradually with the increase in initial oil concentration up to 2 g/L then it decreased with further increase in the initial oil concentration. The increase in adsorption capacity with initial oil concentration was attributed to the increased collision rate of oil droplets with the surface while when the oil concentration increases further the collision rate between oil droplets becomes higher than that occurring between the droplets and the surface. On the contrary, the removal efficiency decreased with the increase in initial oil concentration (from 91.4% to 69.3%) when the concentration increased from 0.5 to 3 g/L. The highest adsorption capacity was found to occur at pH in the range 5–8. Increasing the adsorbent dose from 0.5 to 2 increased the capacity from 13.5 to 22.3 and the efficiency from 94.3% to 98.7% while these values decreased after increasing the dose to 3 g.

Other oil adsorbing agricultural-based materials that were investigated by some other researchers included raw and chemically-treated palm fibers [16], banana peels [17], flax fibers [18] and sawdust [19]. Abdelwahab et al. [16] tested treated and un-treated palm fibers and three types of oils namely; crude oil, diesel oil and vegetable oil. It was found that the maximum adsorption capacity was 24,000; 22,000 and 16,000 mg·oil/g adsorbent for diesel oil, crude oil and vegetable oil, respectively. The high adsorption capacity with the diesel oil was attributed to its high viscosity compared to the raw and vegetable oil. The removal efficiency increased with increasing the dose up to 0.2 g then it remained nearly unchanged up to 0.5 g while the adsorption capacity exhibited an opposite effect, that is, remained nearly unchanged up to 0.2 g then decreased rapidly at 0.3 g then remained unchanged. The achieved maximum adsorption capacity in their study was 35,000 mg·oil/g adsorbent when the dosage was 0.2 g. Alaa El-Din et al. [17] studied the effect of the particle size of banana peels on oil removal from water (gas oil and crude oil). It was found that the sorption capacity increased as the particle size decreased and reached a maximum value at 0.36 mm after which the sorption capacity decreased with further decrease in the particle size. The maximum sorption capacity reached 5,310; 6,350 and 6,630 mg·oil/g adsorbent for gas oil, 1-d weathering and 7-d weathering, respectively. This enhancement was attributed to the increase in surface area. Additionally, the sorption capacity increased with increasing water salinity and reached a maximum value at 3.5% salinity. Mahmoud [18] tested raw, chemically-treated, and thermally-treated flax fibers for the removal of used motor oil from artificial seawater (3.5% NaCl). It was found that the sorption capacity of water, oil and oil/water mixture was 16,450; 15,230 and 13,250 mg·oil/g adsorbent for raw flax, 1,210; 26,820 and 24,540 mg·oil/g adsorbent for chemically-treated flax, 20,100; 21,150 and 17,420 mg·oil/g adsorbent for thermally-treated flax, respectively. Increasing the sorbent dose from 0.5 to 1 g resulted in an increase in the removal ratio from 61.37% to 99.99% which was attributed to the increase in the sorption sites in the fiber. On the contrary, increasing the dose from 1 to 3 g resulted in a decrease in the sorption capacity which was attributed to the aggregation of the sorption sites. When the initial oil concentration was varied from 10 to 35 mL/L, the removal ratio decreased from 99.98% to 71.41% and the adsorption capacity increased from 9,830 to 24,400 mg·oil/g adsorbent. Hussein et al. [19] tested modified sawdust (acid treatment) for oil removal (crude oil with a low viscosity and lubricating oil with a high viscosity) from artificial seawater.

The adsorption capacity was larger by about 440 mg/g for the low viscosity oil compared to the high viscosity oil after 60 min while the opposite occurred after 90 min.

It may be concluded from the above studies that several factors affect the oil adsorption characteristics such as (i) the adsorbent pre-treatment method, (ii) the pH value, (iii) the oil viscosity, (iv) the adsorbent dose, (v) the type of water and the method of oil emulsification and (vi) the initial oil concentration. Additionally, the use of agricultural wastes as adsorbents exhibited a promising performance for oil removal from water. However, there is an interaction among these factors which makes understanding the adsorption mechanisms more complex and consequently, more research is still needed. Accordingly, in the present study, three agricultural wastes namely: rice husk (RH), sawdust (SD) and sugarcane bagasse (SCB) were selected and tested for oil removal from raw and artificial seawater. It is worth mentioning that these wastes are available in Egypt with large amounts and may be considered as cheap adsorbents. Egypt produces about 6 million tons of rice annually, as reported by El-Shahway et al. [20] and about 16 million tons of sugarcane as reported by Michael and Moussa [21]. It is worth mentioning that RH represents about 20% (one-fifth by weight) of the rice production as reported by Kumagai et al. [22]. In other words, about 1.3 million tons of RH are produced every year. Additionally, about 30% can be produced as bagasse waste from sugarcane processing as reported by Mahmud and Anannya [23], that is, 4.8 million tons of bagasse can be produced in Egypt every year. The current study investigated the effect of different experimental conditions on the adsorption characteristics of rice husk, sawdust and sugarcane bagasse. Activated carbon was included in the tests conducted in the current study to be considered as a reference material to compare with. The experimental conditions included the effect of initial adsorbate (oil) concentration, adsorbent dosage, contact time, agitation time, and treatment method. In addition, the interaction between oil and salinity was investigated through testing real seawater mixed with oil. Several adsorption isotherms and kinetics models are also investigated in the current study.

2. Materials and methods

2.1. Raw seawater

The raw seawater was collected from the Mediterranean Sea at the beach of Damietta city, Egypt. The raw seawater was characterized by different physical and chemical examination. The measured parameters were turbidity, electrical conductivity, temperature, pH, total dissolved solids, total suspended solids, calcium (Ca^{++}), chloride (Cl^{-}), and magnesium (Mg^{++}), Table 1.

2.2. Adsorbents

The agricultural wastes used in this study include: rice husk (RH), sawdust (SD) and sugarcane bagasse (SCB). Rice husk was collected from a local rice mill, sawdust was collected from a waste disposal location in Damietta city, and sugarcane bagasse was collected from a waste disposal location in Mansoura city. All samples were washed with tap water and eventually with distilled water to remove any dust and/or impurities. After washing, the samples were dried in a furnace at 105°C until the sample mass did not change. The materials were grinded well and sieved by mechanical sieve shaker to obtain the average size of 600–1,000 μm diameter. After that, all samples were stored in dried plastic bottles. Activated carbon (AC) was included in the tests to be considered as a reference case to compare with the tested agricultural wastes. All adsorbents were characterized using the following methods:

- Scanning electron microscopy: The morphology of the tested adsorbents was examined by a scanning electron microscope (SEM), model JEOL JSM-6510LV (Japan), Faculty of Science, Mansoura University. The SEM images were recorded at an accelerating voltage of 20 kV and a magnification of 2,000.
- Brunauer–Emmett–Teller (BET): BET was used to measure the morphological properties such as surface area, pore size distribution, and pore volume of the adsorbents. BET was performed using liquid nitrogen at 77.03 K (–196°C). This test was conducted at the Faculty of Science, Cairo University.
- Fourier-transform infrared spectroscopy (FTIR): FTIR was used to characterize the morphology of adsorbents. It is used to identify the functional groups on the surface of the adsorbents. The wave numbers ranged from 4,000 to 400 cm^{-1}. The adsorbents were analysed using the FTIR-4100 spectrophotometer in the Faculty of Science, Damietta University.

2.3. Tested oils

Two types of oil namely; used motor oil (UMO) and crude oil (CO) were tested in the present study to investigate the oil sorption and oil adsorption capacity. The UMO was obtained from a motor service workshop while the CO was purchased from sham OEMIX multi-grade motor oil, which is suitable for diesel and natural gas engines SAE-50. Table 2 shows the density and viscosity of the UMO and CO measured in the Laboratory of Oil Perg Company located in the New Damietta.

2.4. Batch experiments

Batch experiments were carried out to determine the oil sorption and adsorption capacity of the four tested

Table 1
Raw seawater analysis

Parameter	Avg. value
Total dissolved solids, ppm (mg/L)	35,500
Total suspended solids, ppm (mg/L)	240
pH	8.2
Temperature, °C	27.8
Electrical conductivity, μS/m	3,886.2
Turbidity, NTU	80.2
Calcium (Ca^{++}), ppm (mg/L)	474
Magnesium (Mg^{++}), ppm (mg/L)	965
Chlorides (Cl^{-}), %	2.16

adsorbents; RH, SD, SCB, and AC. The effect of different factors including adsorbent material, type of oil, initial adsorbate (oil) concentration, contact time, adsorbent dosage, agitation time, salinity, metal ions concentration, and the type of modification (acid or/and alkaline treatment) were studied in these experiments. The oil sorption removal was investigated by varying one factor while keeping the other factors constant at oil concentration 10 g/L, sorbent dose 6 g/L, contact time 30 min, and shaking at 115 rpm for 15 min. The experiments were conducted in the following sequence: (1) a net (mesh) made of aluminium material was attached to the bottom and side walls of a 250-mL beaker, (2) distilled water and/or raw seawater was added to the beaker. (3) The oil sample was added to the beaker with concentration 2, 5, 10, 20, 30, and 40 g/L. (4) The adsorbent dose was added to the solution. (5) The mixture was mixed and shacked at a speed of 115 rpm for 15 min in a water bath. (6) After agitation, the mixture was left for 30 min as a contact time, then, the mesh containing adsorbent was removed from the beaker. The mesh was allowed to drip off for 15 min under gravity, according to the ASTM standards [24] as reported by Bazargan et al. [25] and Hussein et al. [19], then it was maintained in the furnace at 105°C to remove the remaining moisture. After draining and drying, the mass of the adsorbent was measured by a digital balance with accuracy (±0.001 g). The measured mass was used to determine the adsorption capacity and oil sorption. All tests were carried out at the room temperature and the measurements were conducted for three samples with a mean absolute deviation (deviation from sample to sample) of 15% (the average value of the three samples was used in the current study). The mass of the adsorbed oil was the difference between the mesh containing the adsorbent after drying and the weight of the mesh with the adsorbents before the experiment. The adsorption capacity and the oil removal efficiency of the adsorbent was calculated using Eqs. (1) and (2), respectively, Abdelwahab et al. [16]. The systematic flow chart of batch adsorption experimental conditions is shown in Fig. 1 for CO and UMO on raw sweater and distilled water.

$$\text{Oil adsorption capacity}\left(q_e\right),\left(\text{mg/g}\right) = \frac{\text{Mass of oil adsorbed}\left(\text{mg}\right)}{\text{Mass of adsorbent}\left(\text{g}\right)} \quad (1)$$

$$\text{Oil removal efficiency}\left(S\right),\left(\%\right) = \frac{\text{Mass of oil adsorbed}\left(\text{g}\right)}{\text{Initial mass of oil}\left(\text{g}\right)} \times 100 \quad (2)$$

Table 2
Measured density and viscosity of the oils used in the current study

Parameter	CO	UMO
Specific density, g/cm^3	0.875	0.9
Viscosity at 40°C, cSt	63	98

3. Results and discussions

3.1. Adsorbents characterization

3.1.1. SEM analysis

The adsorbent surface morphology was analysed using the SEM with magnifications 250 as depicted in Fig. 2. Fig. 2a depicts the texture of the RH which shows a well-ordered protrusions and honeycomb-like structure (pores) which can enhance the penetration of the adsorbate into the pores and consequently may help enhance the performance of the adsorption process. The morphology of the SD shown in Fig. 2b exhibits a porous structure, which looks like parallel fibers or thin straws. The SEM images of the SCB shown in Fig. 2c demonstrate that there are several fibers with irregular shape, it looks like plant leaves. It can be observed from Fig. 2d that the surface morphology of the AC has a completely different structure, which is a highly porous structure with a wide range of pore size. In conclusion, the surface morphology of the four tested adsorbents exhibited completely different structure.

3.1.2. BET analysis

BET analysis was used to obtain the surface area, total pore volume, and average pore diameter. The surface area of RH, SD, SCB and AC are found to be 174.3, 46.2, 61.8, and 742.6 m^2/g, respectively. This may provide more active adsorption sites leading to the adsorption of more oil molecules. The measured morphological properties of the adsorbents used in the current study include surface area, total pore volume and average pore diameter as summarized in Table 3.

3.1.3. FTIR spectra analysis

The FTIR was performed for the raw and chemically-treated RH, SD, SCB and AC as shown in Fig. 3. The interested reader is referred by Nandiyanto et al. [26] for more details about how to read and interpret the FTIR spectroscopy. Fig. 3a shows the FTIR spectrum of the raw RH, RH treated with HCl and RH treated with NaOH and HCl. The bands in the region of 3,417.24; 3,433.64 and 3,420.14 cm^{-1} indicate the presence of single-bond O–H group present in cellulose, hemicellulose, and lignin for RH, RH-HCl, and

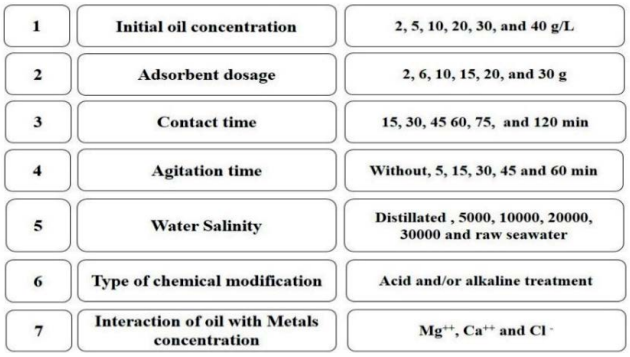

Fig. 1. Systematic flow chart of batch adsorption experimental conditions.

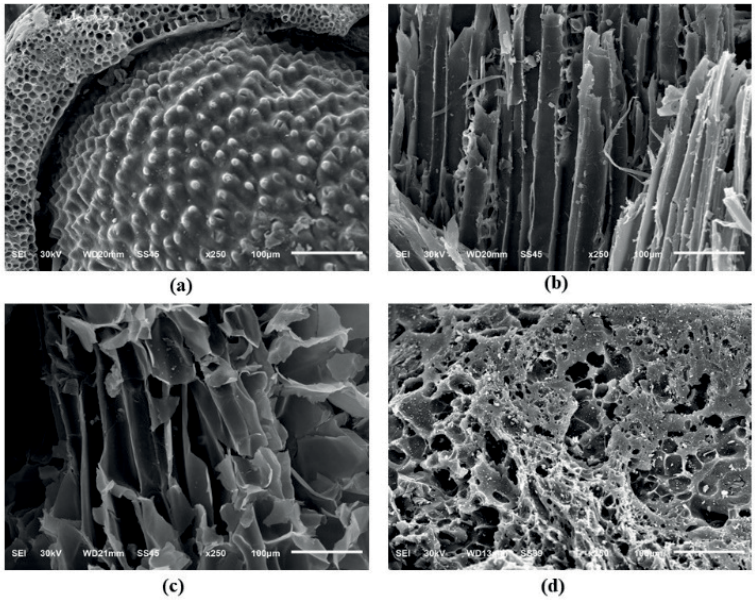

Fig. 2. Scanning electron microscopy images of (a) rice husk, (b) sawdust, (c) sugarcane bagasse, and (d) activated carbon.

Table 3
Morphological properties of the tested adsorbents

Parameter	Unit	RH	SD	SCB	AC
Surface area	m^2/g	174.337	46.152	61.8112	742.565
Total pore volume	cm^3/g	0.1787	0.0755	0.10027	0.45098
Average pore diameter	nm	2.0511	3.2736	3.2444	1.21467

RH-(NaOH & HCl), respectively. The bands at 2,924.52; 2,919.7 and 2,920.66 cm^{-1} are assigned to C–H asymmetric stretching of alkanes for RH, RH-HCl, and RH (NaOH and HCl), respectively. The bands at 2,134.81 cm^{-1} represents strong C=N for RH-HCl. Furthermore, the bands at 1,731.76; 1,725.25 and 1,724.05 cm^{-1} correspond to the stretching of a carbonyl group C=O for RH, RH-HCl, and RH-(NaOH & HCl), respectively, that may be attributed to the hemicellulose and lignin aromatic groups [27]. The bands at 1,631.48; 1,639.2 and 1,646.91 cm^{-1} represent C=C bending aromatic group and the bands at 1,375; 1,380.78 and 1,377.89 cm^{-1} are assigned to the C–H bending. In addition, the bands at 1,240; 1,264.11 and 1,268.93 cm^{-1} correspond to C–N stretching. The bands at 1,108.87 cm^{-1} correspond to the C–O anti-symmetric stretching for RH-(NaOH & HCl) and the bands at 1,099.23 and 1,031.73 cm^{-1} correspond to Si–O–Si stretching for RH and RH-HCl.

The main component of SD is cellulosic biomass which defines the generic characteristics in the spectrum of a generic oxygenated hydrocarbon [28]. The peaks of 3,384; 3,367 and 3,366 cm^{-1} appeared in SD, SD-HCl, and SD-(NaOH & HCl) due to the O–H stretching vibrations of phenol and alcohol, which demonstrated a broad band between 3,000 and 3,600 cm^{-1} as shown in Fig. 3b. The absorption peaks between 3,600 and 4,000 cm^{-1} were pronounced and peaks almost vanished, which may be attributed to the free –OH stretching vibrations. The peaks observed at 2,909; 2,907 and 2,904 cm^{-1} were assigned to C–H stretching of alkyl group and the peak at 1,729; 1,728 and 1,725 cm^{-1} were due to the presence of C=O stretching vibrations of ketones, esters and aldehydes for SD, SD-HCl, and SD-(NaOH & HCl), respectively. The peaks observed at 1,602; 1,647 and 1,656 cm^{-1} for SD, SD-HCl, and SD-(NaOH & HCl) were due to aromatic ring of lignin, while the peak at 1,056; 1,057 and 1,058 cm^{-1} were assigned to C–O–C or C–O stretching of ether groups of lignin, cellulose and hemicellulose.

Fig. 3c depicts for the SCB that there are hydroxyl group (–OH), carbon–hydrogen bonding (C–H), carbon–oxygen bonding (C–O), carbon–oxygen double bonding (C=O), aromatic rings (C–H), and carbon–oxygen–hydrogen bonding (C–OH) as also reported by Abdul Hamid et al. [29]. The bands of raw SCB appearing at 3,413.39 and 2,912.95 cm^{-1} was assigned to stretching vibrations of hydroxyl groups (–OH) and carbon-hydrogen bonding (C–H) in lignin, hemicelluloses and cellulose, respectively. The bands of 2,141.56; 1,728.87 and 1,640 cm^{-1} are assigned to carbonyl group, carbon–oxygen double bonding (C=O), and C=C in lignin, respectively. The bands at 1,054 and 1,160 cm^{-1} represent primary and secondary –OH groups. Some changes in frequency and intensity bands are observed in SCB modified with HCl and NaOH-HCl. The –OH and C–H groups of SCB modified with HCl and NaOH & HCl appear at bands 3,417.24; 3,438.46; 2,918.73 and 2,924.52 cm^{-1}. The carbon-oxygen double bonding (C=O) disappeared in the SCB modified with HCl.

The FTIR of commercial-AC are shown in Fig. 3d. The wavenumber at 3,405.67 cm^{-1} represented the hydroxyl groups (–OH). The stretch vibration of C–H alkane was observed at peak 2,920.66 cm^{-1}. The peak at 1,727.91 cm^{-1} represented the stretch vibration of C=O group, while the peak at 1,588.09 cm^{-1} indicated the stretch vibration of C=C aromatic. The O–H bending was represented at peak 1,339.32 cm^{-1}, the C–O–C stretching was represented at peak

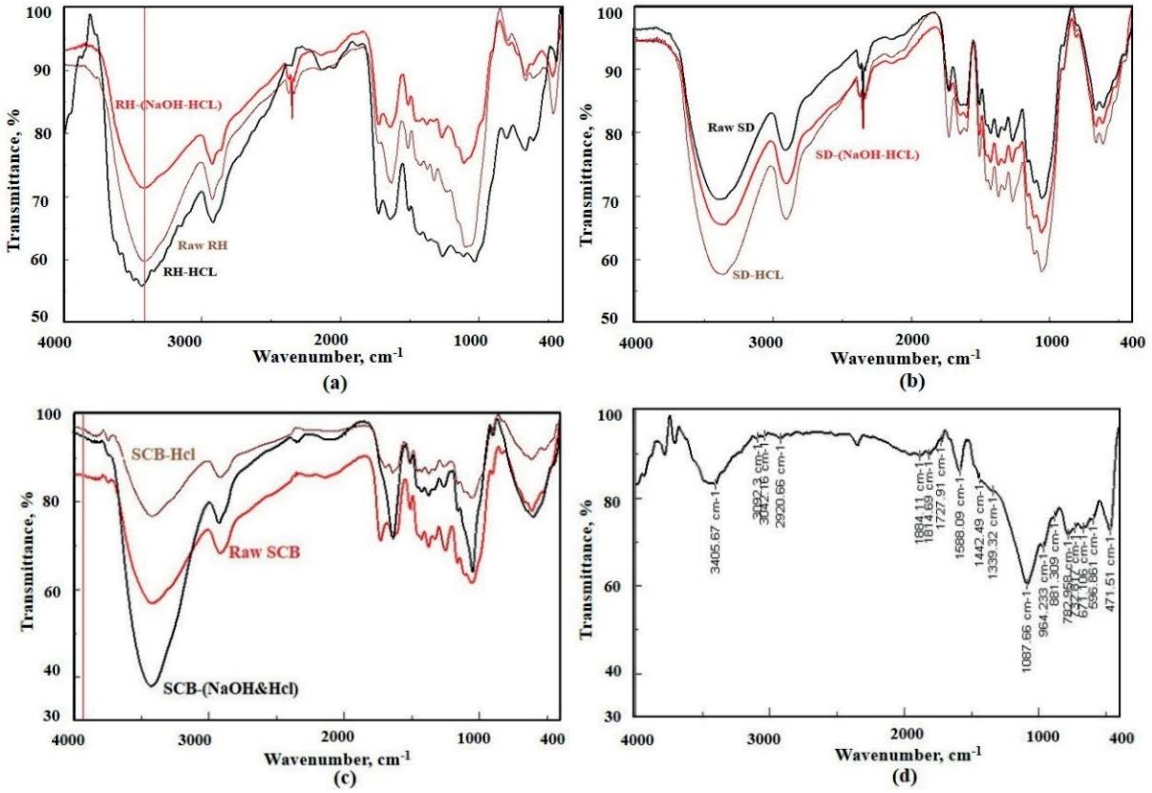

Fig. 3. Fourier-transform infrared spectra of the raw and modified (a) rice husk, (b) sawdust, (c) sugarcane bagasse, and (d) activated carbon.

1,087.66 cm^{-1}. According to Ehsan et al. [30], these peaks are considered the main functional groups on the surface of the AC can be expressed as hydroxyl and carboxylic anhydride groups.

3.2. Parametric study

3.2.1. Effect of initial adsorbate (oil) concentration

The influence of initial oil concentration was investigated at a fixed adsorbent dose of 6 g/L and contact time of 30 min for each type of oil and raw seawater and distilled water. Fig. 4 depicts the effect of initial oil concentration (range 2–40 g/L) on the oil sorption removal while Fig. 5 shows the effect on the adsorption capacity. It was observed that the oil sorption removal decreased rapidly when the oil concentration was increased from 2 to 20 g/L, while it decreased slowly when the oil concentration increased from 20 to 40 g/L.

Fig. 5 shows that the adsorption capacity increased rapidly when the initial oil concentration increased from 2 to 20 g/L then it remained approximately constant. For the UMO, the adsorption capacity at equilibrium state occurring at initial concentration of 20 g/L (Fig. 5a and b) was 1,729; 1,351; 889 and 616 mg·oil/g adsorbent, respectively for AC, RH, SCB and SD with distilled water while it was 1,936; 1,510; 1,067 and 905 mg·oil/g adsorbent with raw seawater. For the CO (Fig. 5c and d), the equilibrium adsorption capacity (at initial oil concentration of 20 g/L) was 1,635; 1,318; 832 and 595 mg·oil/g adsorbent, respectively for AC, RH, SCB, SD with distilled water while it was 1,641; 1,214; 934 and 721 mg·oil/g adsorbent with raw seawater. In addition, it is observed that the adsorption behaviour of each adsorbent is different, where the highest adsorption capacity occurred with the AC followed by RH, SCB, and SD. The results indicated that for the UMO the adsorption capacity was slightly higher in seawater compared to distilled water for AC and RH (about 12% difference) while the adsorption capacity of SCB and SD in raw seawater were 20% and 46.9% higher compared to the distilled water. In other words, there is no difference between distilled and raw seawater for some adsorbents (AC and RH) while the difference could be large for some others (SCB and SD). On the contrary, for CO, the difference between distilled water and seawater was less than 12% for AC, RH and SCB while it was 21.2% for SD. In conclusion, in batch experiments care should be taken when distilled water is used in the experiments. The results demonstrated also that RH achieved adsorption capacity close to those obtained with the AC, for example, the difference was about 22% with UMO regardless the type of water while it was 19.4% and 26% with CO, respectively for distilled water and raw seawater.

3.2.2. Effect of adsorbent dose

Fig. 6 shows the effect of adsorbent dose (2–30 g/L) on the oil sorption removal while Fig. 7 depicts the effect of the dose on the adsorption capacity. The results indicated

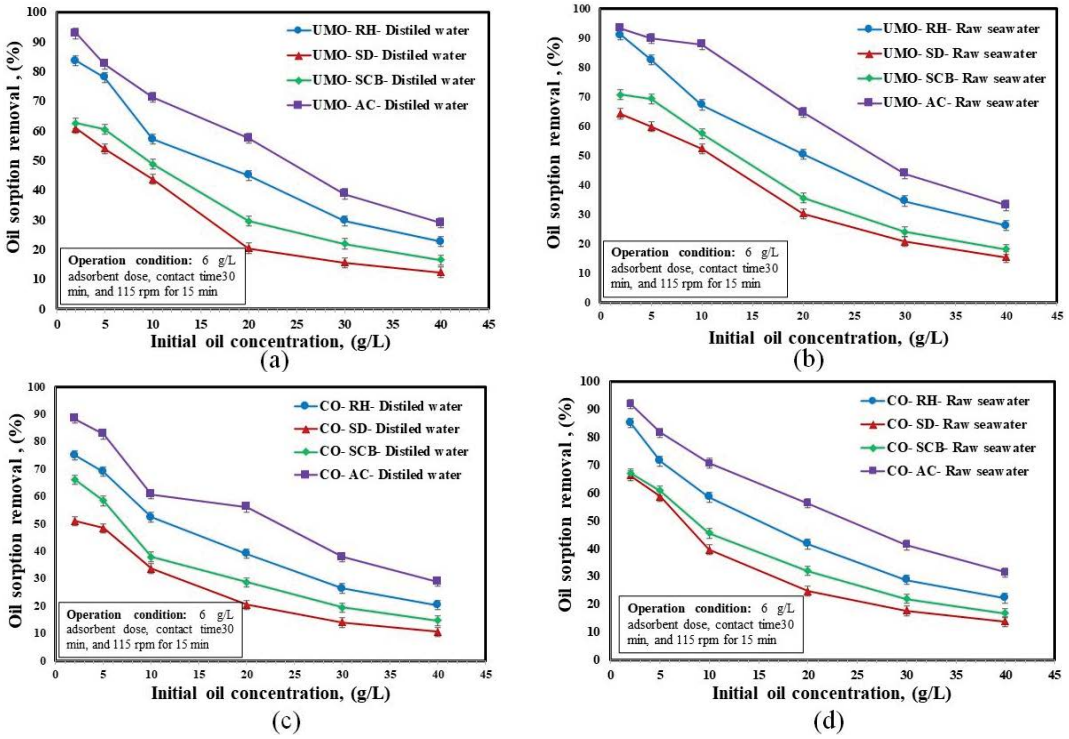

Fig. 4. Effect of initial oil concentration on oil sorption removal (%).

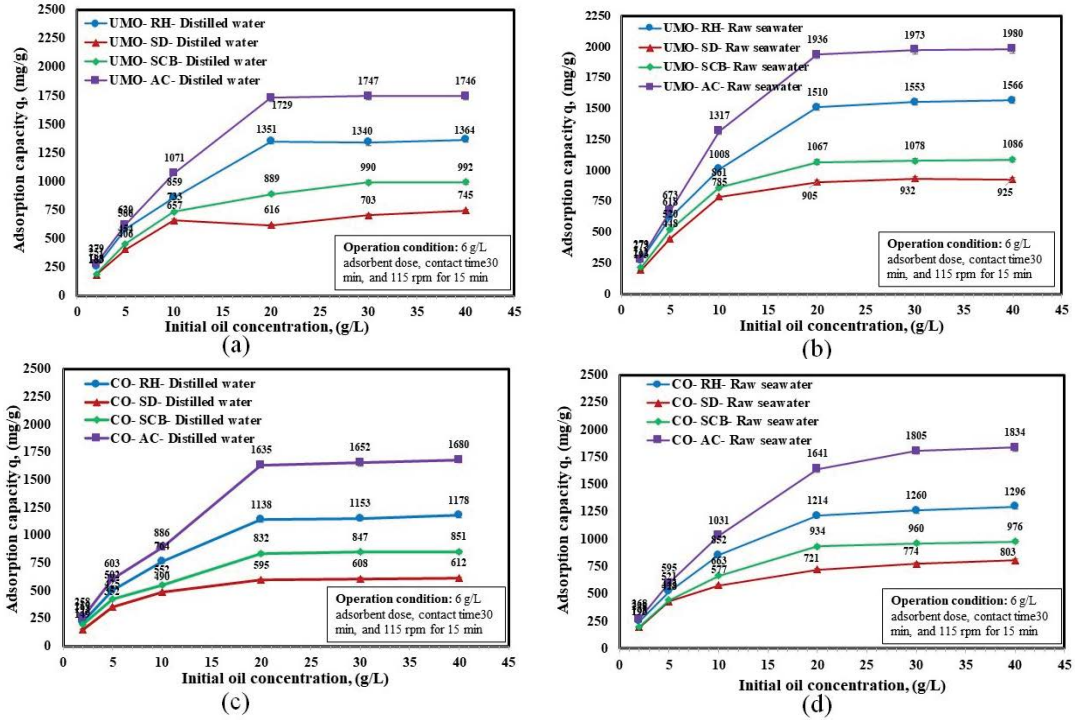

Fig. 5. Effect of initial oil concentration on adsorption capacity, (mg/g).

that as the adsorbent dose increases, the oil sorption removal increased rapidly up to a dose of about 5–10 g/L after which the oil sorption removal has increased at a lower rate (remained constant in some cases) compared to the doses below 5–10 g/L. In contrast, Fig. 7 illustrates that the curves of the adsorption capacity exhibited an opposite trend,

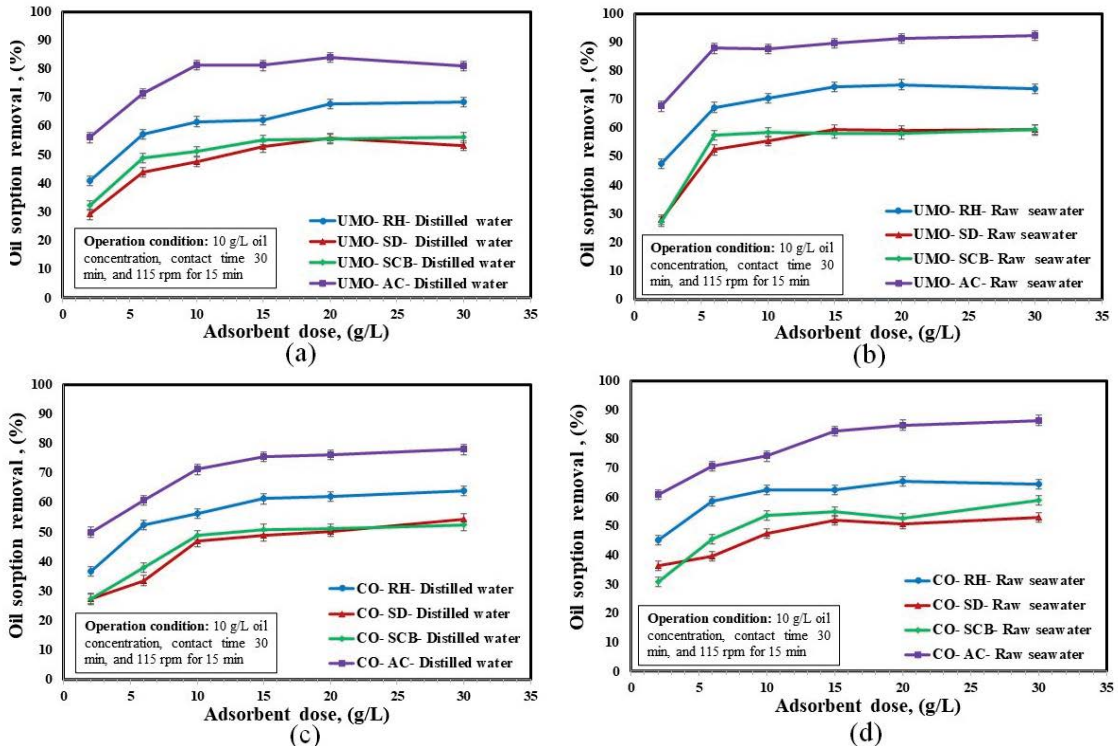

Fig. 6. Effect of adsorbent dose on oil sorption removal, (%).

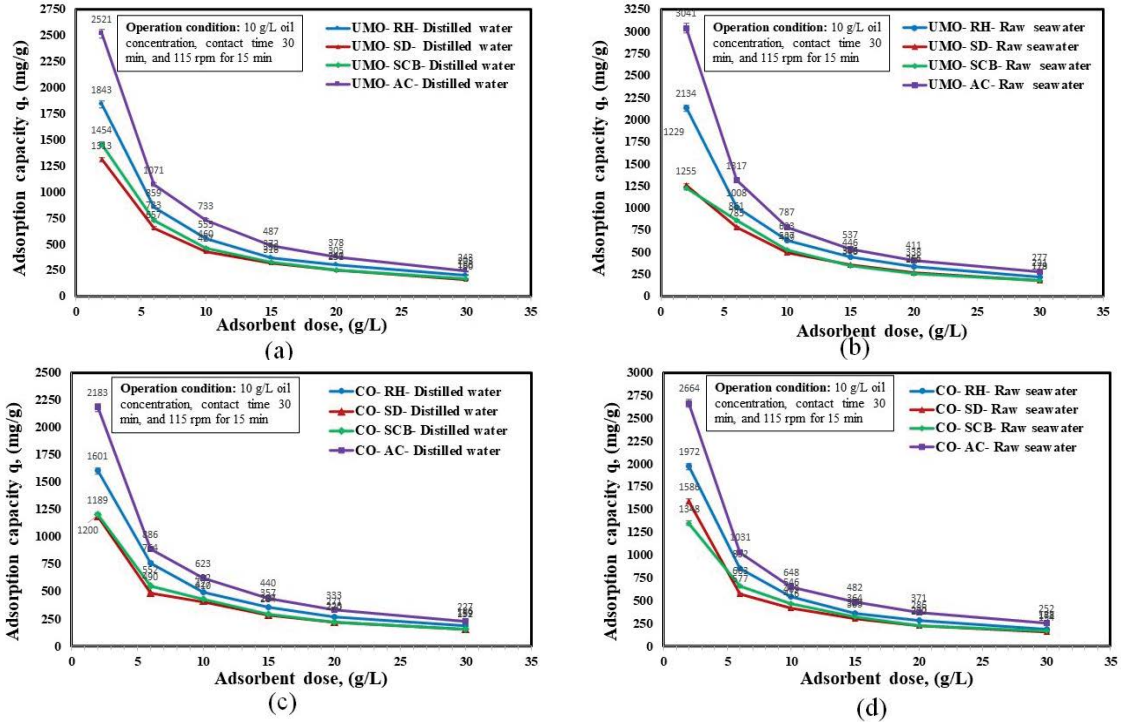

Fig. 7. The effect of adsorbent dose on adsorption capacity, (mg/g).

that is, it decreased rapidly with increasing the dose up to 5–10 g/L then remained nearly unchanged or decreases slightly. The maximum adsorption capacity (at 2 g/L) for the UMO and distilled water was 2,521; 1,843; 1,454 and 1,313 mg·oil/g adsorbent, respectively for AC, RH, SCB and SD while it was 3,041; 2,134; 1,255 and 1,255 mg·oil/g

adsorbent, for raw seawater. For the CO, the maximum adsorption capacity for distilled water was 2,183; 1,601; 1,200 and 1,189 mg·oil/g adsorbent, respectively for AC, RH, SCB, SD while it was 2,664; 1,972; 1,586 and 1,480 mg·oil/g adsorbent for raw seawater. The increase in oil sorption removal and the decrease in adsorption capacity with increasing the adsorbent dose may be attributed to the greater number of active sites on the adsorbent surface, which help oil molecules to penetrate into these active sites as reported by Razavi et al. [31]. The decrease in the adsorption capacity may be due to the higher existing unsaturated sites during adsorption process as explained by Ngah and Hanafiah [32]. Similar results were reported in literature, for example, [16,31,33]. The results demonstrated that the highest adsorption capacity was achieved with AC followed by RH and the difference was 26%–30% for the two types of oil and water. For the UMO, the highest difference between raw seawater and distilled water was 20.2% for AC and 15.8% for RH while for the CO, the highest difference was 32.2% for SCB and ranged from 22% to 24.5% for AC, RH and SD.

3.2.3. Effect of contact time

Fig. 8 shows the effect of contact time (15–120 min) on oil sorption removal for CO and UMO at a fixed adsorbent dose of 6 and 10 g/L initial oil concentration and shacked for 15 min at 115 rpm. The figure demonstrates that oil sorption removal as a function of contact time can be divided into two phases; the first phase is the primary fast removal stage due to the fact that high amount of oil can be adsorbed and thus most of the available sites become occupied with oil. The second phase is the slow sorption removal stage and it occurs before equilibrium state Abdelwahab et al. [15]. Additionally, the figure shows that the oil sorption removal increased with increasing contact time until it reached the maximum adsorption capacity. It can also be seen that the rate of oil removal was very high in the beginning (first 15 min) then it increased gradually and became almost steady with the same trend as shown in Fig. 8a–d. The rapid oil sorption removal rate at the beginning of contact may be attributed to the high number of vacant surface binding sites for oil adsorption. The percent CO oil sorption removal in the first 15 min for seawater was 58.2%, 42.7%, 36.4%, and 37.1%, respectively for AC, RH, SCB, and SD while for UMO the values were 69.4%, 48.5%, 45.7%, and 41% in the same order. The time needed to reach equilibrium was 30 min for UMO in distilled and raw seawater while for CO, the equilibrium time reached 45 min for distilled water and 30 min for raw seawater. According to the results in Fig. 8, the oil sorption removal percent for the UMO is larger than that for the CO and the AC achieved values higher by 30.1% and 26.6% compared to the RH. In conclusion, the contact time needed to reach equilibrium was 30 min for all cases except the CO with distilled water. Although oils with high viscosity flow with lower velocity and penetrate hardly into the sorbent pores, it attaches well on the adsorbent surface as reported by Razavi et al. [31] and Lim & Huang [34], while the less viscous oil may be attached weakly to the adsorbent surface as reported by Hussein et al. [19] and Razavi et al. [31]. It is worth mentioning that in literature, the contact time required to achieve the highest adsorption capacity varies from study to another and depends on the oil viscosity and other experimental parameters. Accordingly, a wide range of equilibrium contact time can be found in literature. For example, Razavi et al. [31] reported 5 min to reach the high sorption removal while Bayat et al. [35] reported 1, 5 and 90 min for gas oil, light crude oil and heavy crude oil, respectively.

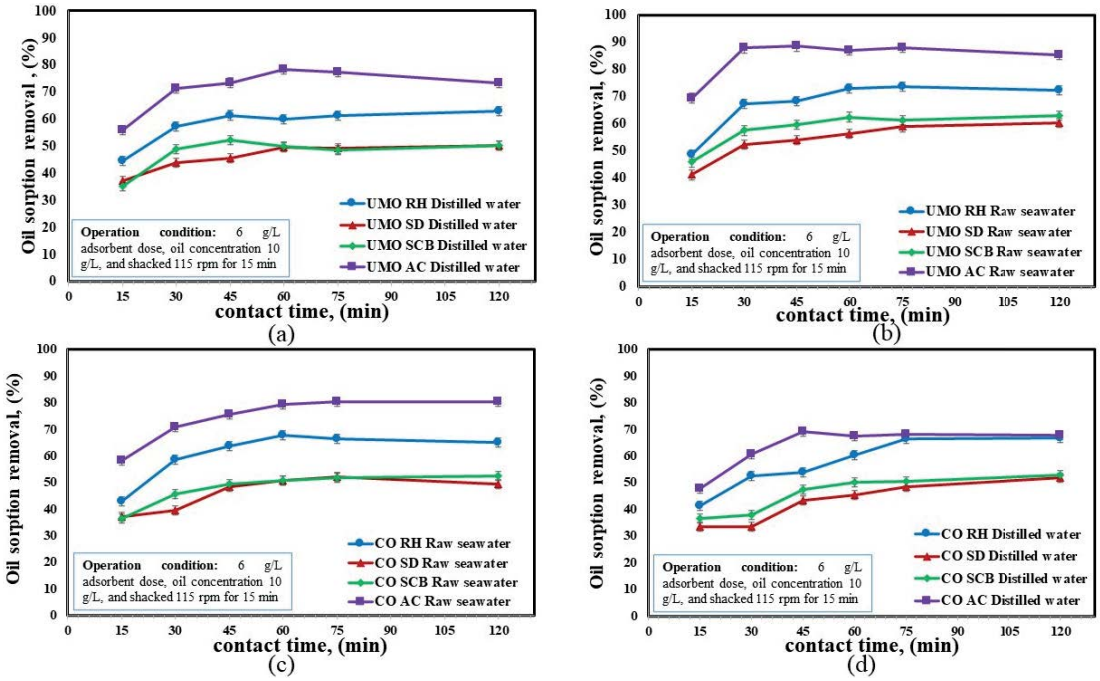

Fig. 8. Effect of contact time on oil sorption removal, (%).

3.2.4. Effect of agitation time

The effect of agitation time (0–60 min) on oil sorption capacity was investigated for a fixed adsorbent dose of 6 g/L, oil concentration 10 g/L and contact time of 30 min. As shown in Fig. 9, the oil sorption percent removal increases with increasing the agitation time with similar trend for all adsorbent with little differences. The results indicated that the most remarkable oil sorption removal occurred in the first 15 min of agitation time after which the oil sorption removal remained approximately constant. The oil sorption removal at 15 min of agitation with UMO in distilled water was 71.4%, 57.3%, 48.9%, and 43.8%, respectively for AC, RH, SCB, and SD while for raw seawater the values were 87.7%, 67.2%, 57.4%, and 52.3%, respectively, for AC, RH, SCB, and SD. The oil sorption removal using CO in distilled water in the first 15 min was 60.7%, 52.4%, 37.9%, and 33.6%, respectively, for AC, RH, SCB, and SD while for the raw seawater the values were 66.7%, 58.5%, 45.5%, and 39.6%, respectively, for AC, RH, SCB, and SD. The percent oil removal was higher in raw seawater by 17.3%–22.8% for the UMO and 9.9%–20% for the CO. Additionally, RH achieved removal ratio slightly lower than activated carbon by about 13% in the CO while it was lower by 19.7%–23.4% in the UMO. Several studies investigated the effect of agitation such as Nechchadi et al. [36] and Olufemi & Otolorin [37] and reported that as the agitation time increases, the oil sorption removal increases due to the increase in the mass transfer rate. The increase in agitation time results in a reduction in the surface film resistance, which allows residual oil to reach the particle surface more easily.

3.2.5. Effect of water salinity

The influence of salinity was performed using distilled water (no salts), synthetic saline water (35% NaCl with distilled water) and raw seawater. Fig. 10 shows the oil sorption removal for the three investigated degree of salinity. The figure indicates that the oil sorption removal is slightly higher in case of raw seawater and synthetic saline water compared to the distilled water. Fig. 11 illustrates the effect of salinity on the oil sorption removal and shows moderate increase with increasing salinity which may be attributed to the premise that the presence of salts may reduce the electrostatic repulsion between the adsorbent and adsorbate surface as reported by Bjelopavlic et al. [38]. The oil sorption removal percents for UMO in distilled water were 71.4%, 57.2%, 48.4%, and 43.7%, respectively for AC, RH, SCB, and SD while for CO the values were 60.7%, 52.3%, 37.8%, and 33.5%, respectively for AC, RH, SCB, and SD. For the raw seawater, the UMO sorption was 87.7%, 67.2%, 57.4%, and 52.3%, respectively for AC, RH, SCB, and SD while for the CO the values were 70.7%, 58.4%, 45.4%, and 39.5%. The oil sorption removal in synthetic saline water is nearly similar to that achieved in raw seawater where the difference between the two types of water was in 2%–7%.

3.2.6. Effect of adsorbent chemical modification

Modification of agriculture waste-based adsorbents using acids and alkali is used to improve the properties of adsorbent surface to enhance the oil sorption removal through modifying the external surface. The experiments

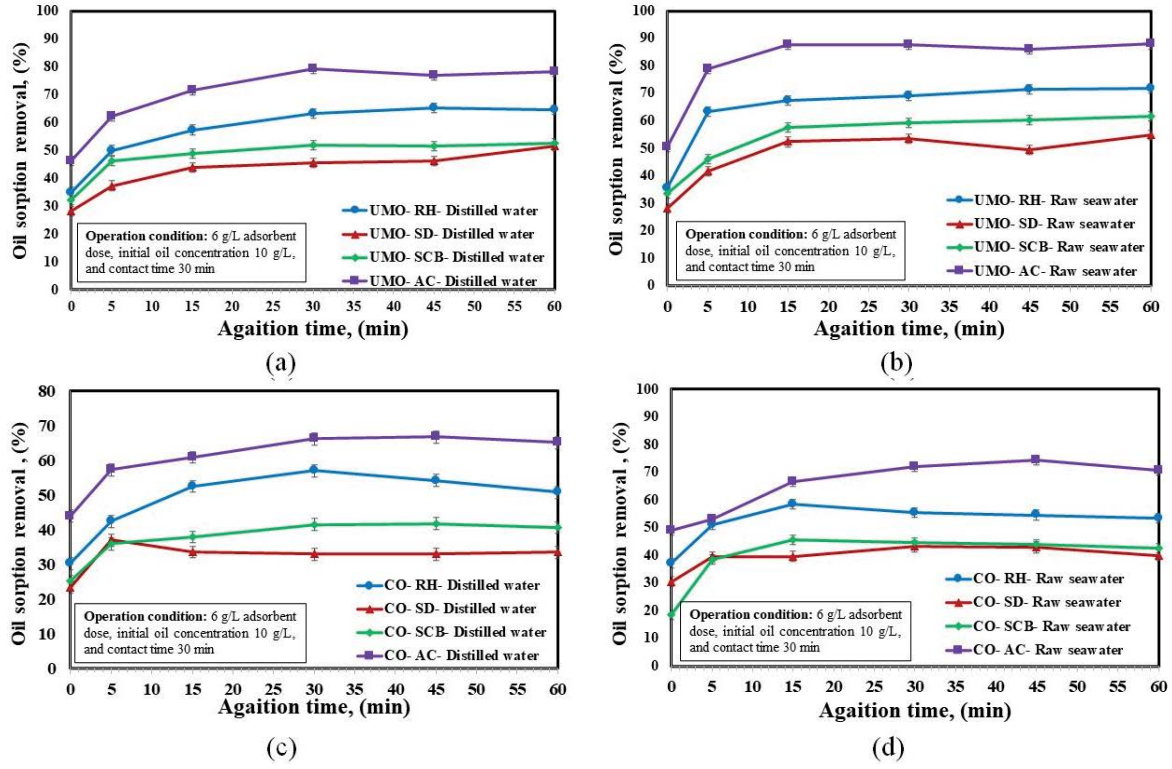

Fig. 9. Effect of agitation time on oil sorption removal, (%).

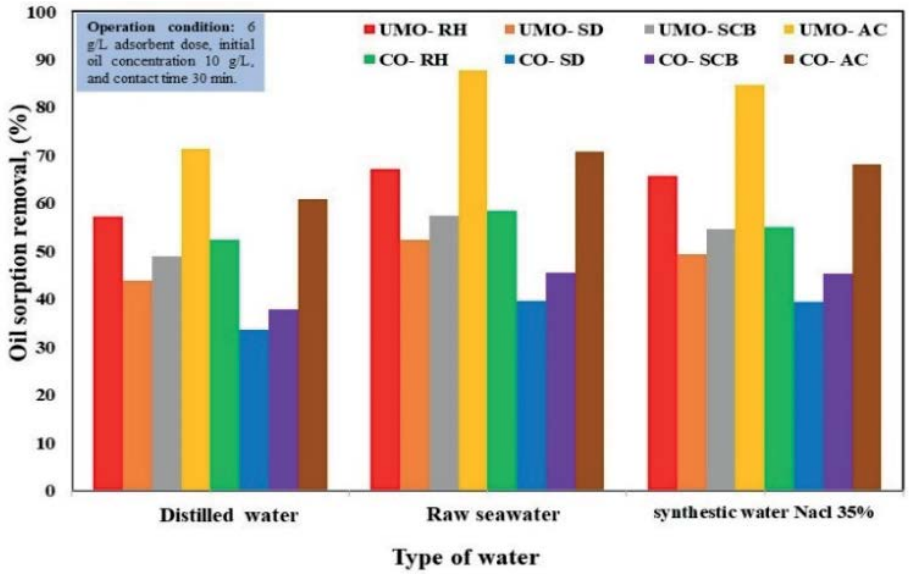

Fig. 10. Effect of type of water on oil sorption removal, (%).

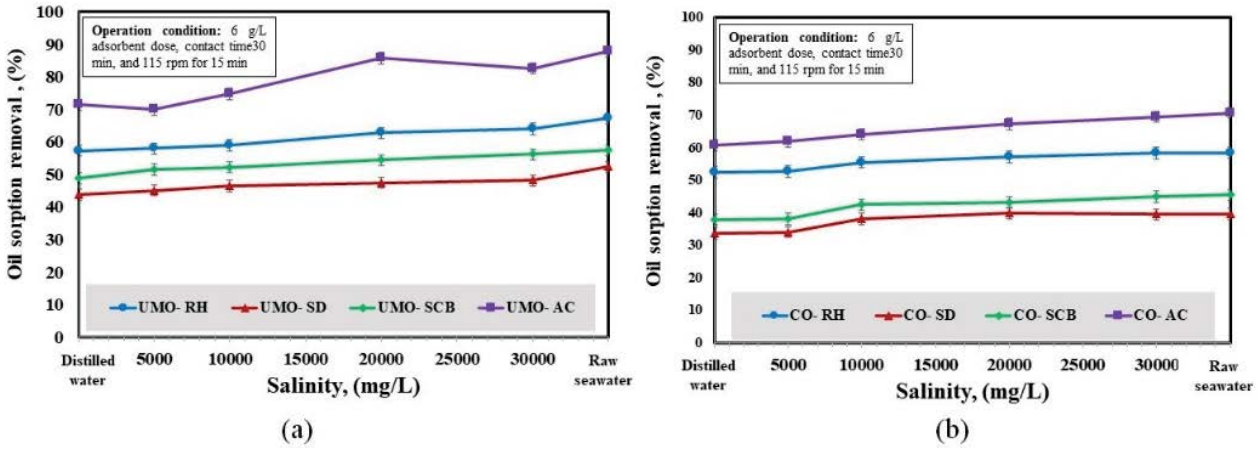

Fig. 11. Effect of salinity on oil sorption removal, (%): (a) used motor oil and (b) crude oil.

were performed for oil concentration 10 g/L, 30 min contact time, 6 g/L adsorbent dosage. HCl and NaOH was used for acid and alkali modification. Fig. 12 shows the oil sorption removal of UMO and CO for distilled water and raw seawater. The UMO sorption removal ratios were slightly higher in the acid modification in distilled water for the RH and SCB where the values were 67.6% and 51.3%, respectively. On the contrary, the CO sorption removal was higher in the raw seawater for SD and SCB where the values were 50% and 50.9%, respectively and in distilled water for SCB 41.6%.

3.2.7. Effect of interaction of oil with some metals in raw seawater

Chemical analysis was conducted to measure the concentration of calcium, magnesium, and chloride in raw seawater. The average concentration of calcium (Ca^{++}), magnesium (Mg^{++}) and chloride (Cl^{-}) for raw seawater was 474 mg/L, 964 mg/L and 2.376%, respectively. Magnesium chloride ($MgCl_2$) and calcium chloride hydrate ($CaCl_2{\cdot}2H_2O$) were used for preparing the sample of synthetic water. The samples contain magnesium, calcium and chloride ions. The experiment was performed for RH (adsorbent dose 6 g/L), oil concentration (10 g/L), magnesium ions concentration 1,000 mg/L, calcium ions concentration 500 mg/L, chloride ions concentration 2.5%, contact time 30 min and shacked 115 rpm for 15 min. Firstly, the concentration of calcium, magnesium and chloride was determined for adsorbent RH using raw seawater, which contains UMO. The calcium, magnesium and chloride sorption removal from seawater were 0.39%, 9.4% and 9.8%, respectively. Secondly, synthetic water contains calcium only were used at the same conditions as above for RH adsorbent. The calcium sorption removal was determined for these samples, which equal 9.7%. Thirdly, synthetic water contains magnesium only was used at the same conditions for RH adsorbent. The magnesium sorption removal was determined for these samples, which equal 54.6%. Fourthly, synthetic water contains

chloride only were used at the same above condition for RH adsorbent. The chloride sorption removal was determined for these samples, which equal 36%. From these results, the oil may be faster in sorption than other metals in seawater. Therefore, the effect of metals can be neglected for oil adsorption.

3.3. Adsorption isotherms

The adsorption isotherms describe the relationship between the amounts of adsorbed sorbent and remaining adsorbate concentration in the solution at equilibrium state, Yun et al. [39]. The adsorption isotherm models of Langmuir, Freundlich, and Temkin were used here to describe the adsorption equilibrium behaviour between the oil (adsorbate) and the used adsorbent materials RH, SD, SCB and AC. The linear and nonlinear equations of these adsorption isotherm models are summarized in Table 4. The evaluation of the isotherms models was based on the R^2 value calculated from linear least square fitting. The main assumptions in all isothermal models are summarized as follows: (i) all sorption sites are equivalent, (ii) the sites are a flat plane, (iii) monolayer coverage of adsorbate and no interactions between adsorbate molecules on the adjacent sites, (iv) each molecule adsorbs on a well-defined site and the adsorbed molecules are localized.

- Freundlich adsorption isotherm is one of the most important empirical correlations used to explain adsorption isotherm. The adsorption process is non-ideal adsorption, which occur onto homogeneous surfaces involving multilayer adsorption and different sites with numerous adsorption energies are involved. The experimental sorption data ($\log q_e$ vs. $\log C_e$) for RH, SD, SCB, and AC are plotted in Fig. 13.
- Langmuir adsorption isotherm was derived based on assumptions which include that the sorption process occurs on homogeneous surface involving saturated monolayer on adsorbent surface, basing on equal sorption activation energy at all sites. The experimental sorption data of Langmuir adsorption isotherm model (C_e/q_e vs. q_e) for RH, SD, SCB, and AC are plotted in Fig. 14.
- Temkin adsorption isotherm was derived based on the assumptions that the heat of adsorption of all molecules reduces linearly during the course of adsorption due to adsorbent–adsorbate interaction in the adsorbing layer, Aharoni and Ungarish [40]. The adsorption reflected by the uniform distribution of binding energies up to

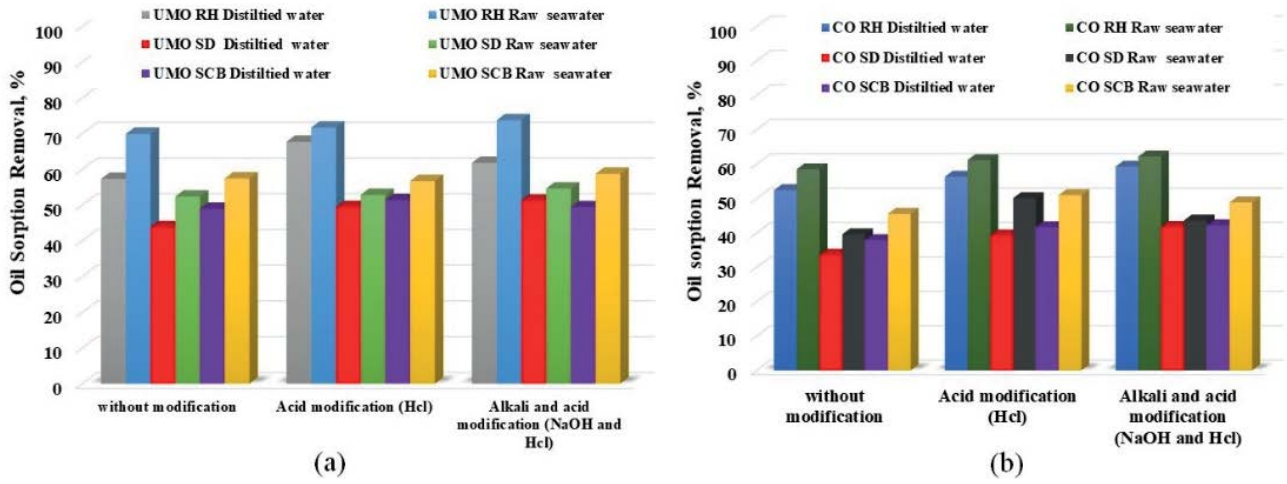

Fig. 12. Effect of surface modification (acid modification and alkali modification) on oil sorption removal, (%) (a) used motor oil in distilled and raw seawater and (b) crude oil in distilled and raw seawater.

Table 4
Equation form of adsorption isotherms modelling

Adsorption isotherm models	Linear equation	Non-linear equation
Langmuir model	$\frac{C_e}{q_e}=\frac{1}{q_{\max}}C_e+\frac{1}{b_{\max}}$	$q_e=\frac{Q_0 bC_e}{1+bC_e}$
Freundlich model	$\log q_e=\log K_f+\left(\frac{1}{n}\right)\log C_e$	$q_e=K_f C_e^{1/n}$
Temkin model	$q_e=B_T\ln C_e+B_T\ln K_t$	$q_e=\frac{R_T}{B_T}\left(\ln C_e k_T\right)$

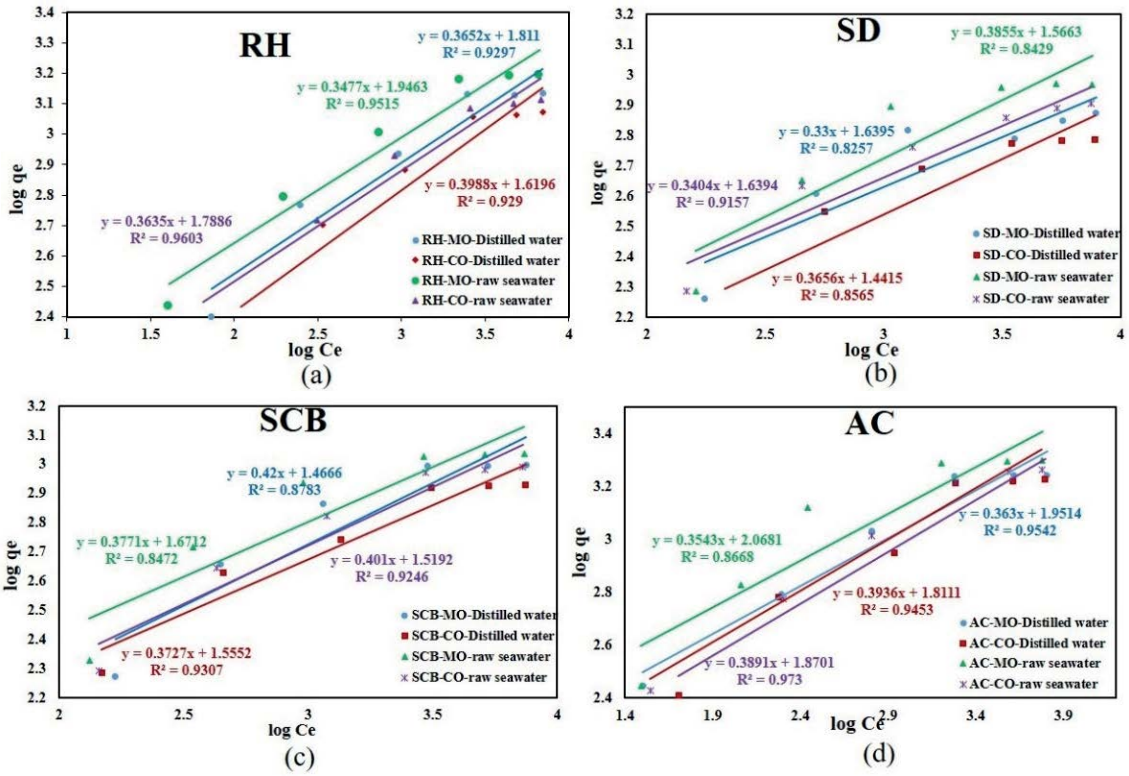

Fig. 13. Freundlich isotherm for rice husk, sawdust, sugarcane bagasse and activated carbon for adsorbed used motor oil and crude oil for distilled water and raw seawater.

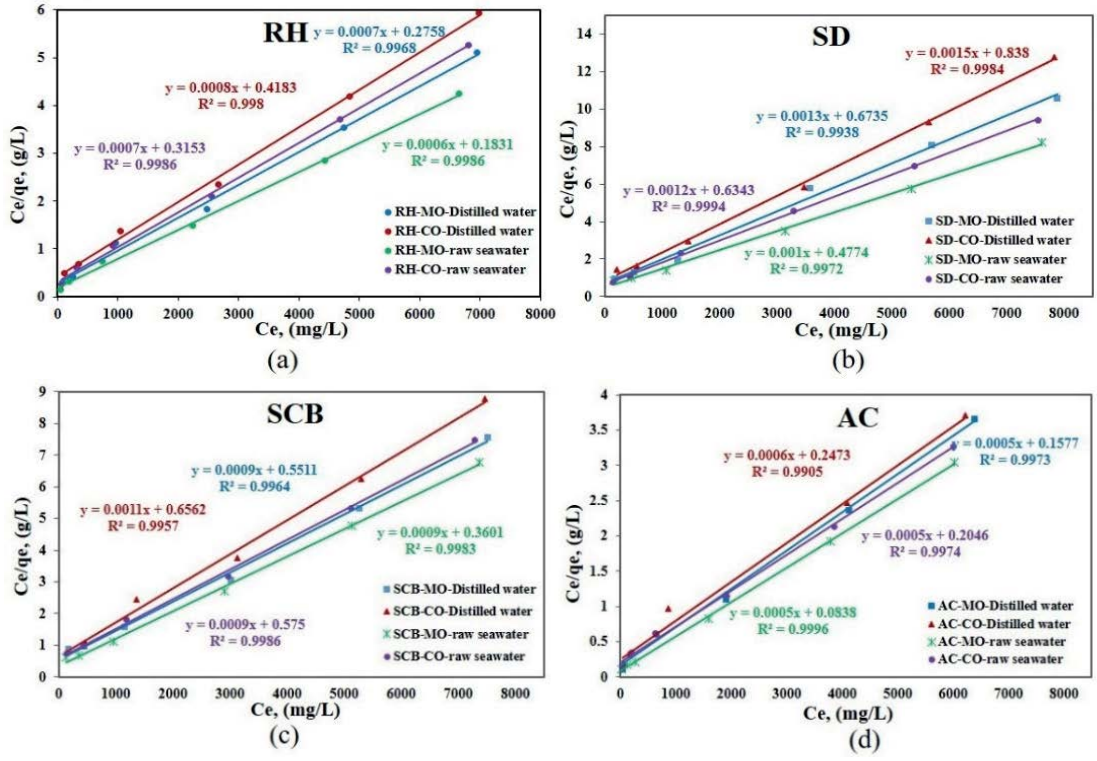

Fig. 14. Langmuir isotherm for rice husk, sawdust, sugarcane bagasse and activated carbon for used motor oil and crude oil for distilled water and raw seawater.

the highest binding energy [41]. The experimental sorption data of Temkin adsorption isotherm model (q_e vs. lnC_e) for RH, SD, SCB, and AC are plotted in Fig. 15.

Applying the Freundlich isothermal model, the values of K_f (g/mg) was found to range from 4.22 to 7.91. The values of the exponent n for RH, SD, SCB, and AC were <1 representing a moderate poor adsorption process. Generally, the values of n in the range 2–10, 1–2, and <1 indicate good, moderately difficult and poor adsorption process, respectively [42]. By applying the Langmuir isothermal model, the values of q_{max} and b can be calculated from the slope and intercept. The maximum adsorption capacity of UMO on RH, SD, SCB, and AC for raw seawater were obtained 1,667; 1,000; 1,111 and 2,000 mg/g, while the maximum adsorption capacity of CO for raw seawater were 1,429; 833; 111 and 2,000 mg/g, respectively. The maximum adsorption capacity of UMO on RH, SD, SCB, and AC for distilled water were obtained 1,420; 769; 111 and 2,000 mg/g, while the maximum adsorption capacity of CO for distilled water were 1,250; 666; 909 and 1,667 mg/g, respectively. In addition, it was observed that the Langmuir constant b (L/mg) ranges from 0.00018 to 0.00597, and the values of R_L are between zero and one confirming that the isotherm is favourable. In addition, applying the Temkin isothermal model, the values of K_T (L/g) ranges from 0.0175 to 0.0909. The B_T (J/mol) is the Temkin isotherm constant linked to the energy parameter, which ranges from are 7.32 to 19.54 for all adsorbents.

The values of each model constant for RH, SD, SCB and AC are summarized in Table 5. The R^2 value of each mode was obtained using the experimental data by plotting the linear equation in each model. The table indicates that the Langmuir isotherm favoured all adsorbents and oil than other isotherms models. The results obtained in the current study show similar trends as the results published by Abdelwahab et al. [15] (modified sugarcane bagasse), [43] (algal biomass), [16] (palm fibers and modified palm fibers), [29] (sugarcane bagasse and banana pith), [31] (modified rice husk), where the experimental sorption data fit with Langmuir isothermal model. However, different trends were reported by Soliman et al. [44] (magnetic wood sawdust), [45] (activated charcoal from sawdust), [33] (coconut coir activated carbon) where all fitted with the Freundlich model.

4. Adsorption kinetics

Generally, adsorption kinetics were used to estimate the time required to reach equilibrium state during the adsorption process and understand the mechanism of the adsorption process. Pseudo-first-order [46], pseudo-second-order [47] and intraparticle diffusion models are used to investigate the adsorption kinetics of oil removal and predict the rate of adsorption. Each model has linear and non-linear procedure but non-linear procedure is a better method to determine the adsorption kinetic parameters are shown in Table 6.

In the pseudo-first-order kinetic model, log (q_e–q_t) is plotted vs. time for RH, SD, SCB, and AC as shown in Fig. 16. The values of K_1 and q_e were estimated from the slope and intercept. In the pseudo-second-order kinetic model the relation between t/q_t and time is plotted in Fig. 17 for RH, SD, SCB, and AC and the values of K_2 and q_e were obtained from the slope and intercept. In the intraparticle diffusion kinetic model, q_t vs. $t^{0.5}$ is plotted in Fig. 18 for

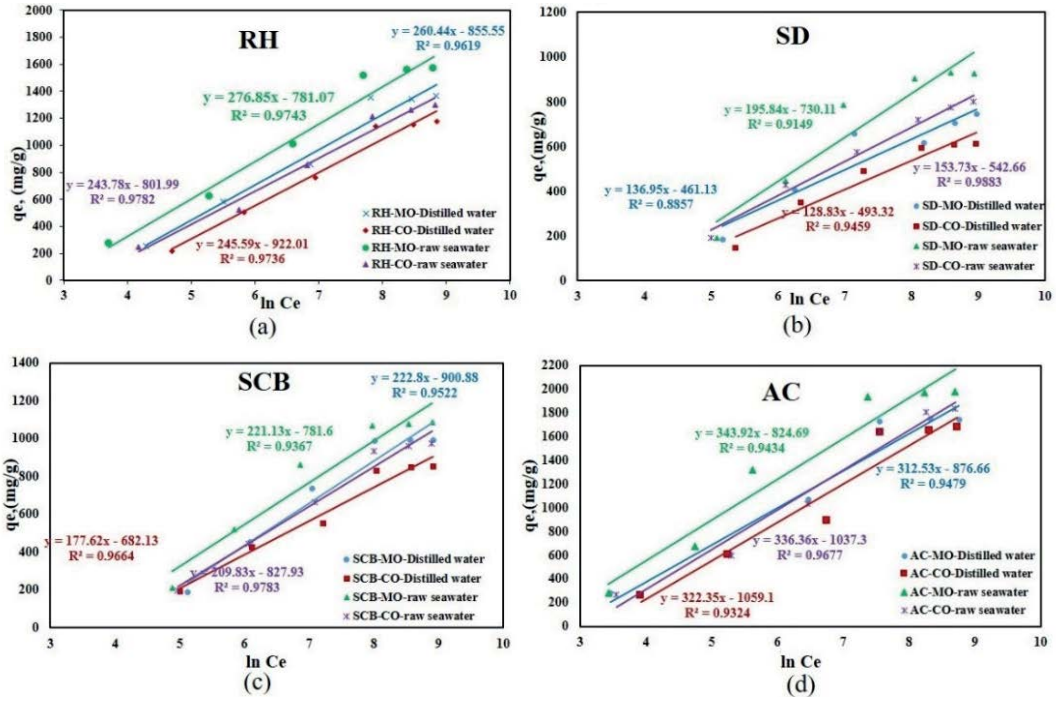

Fig. 15. Temkin isotherm for rice husk, sawdust, sugarcane bagasse and activated carbon for adsorbed used motor oil and crude oil for distilled water, and raw seawater.

Table 5
Freundlich, Langmuir, and Temkin isotherm model parameters and correlation coefficients for UMO and CO onto RH, SD, SCB and AC

Adsorbent type	Freundlich constants			Langmuir constants				Temkin constants			Preferred adsorption isothermal model
	K_f (g/g)	n	R^2	q_{max} (mg/g)	b (L/g)	R^2	R_L	b_T	K_T (L/g)	R^2	
RH-UMO-Distilled water	6.117	0.3652	0.930	1,429	0.0025	0.997	0.0529	9.67	0.0374	0.9619	Langmuir
RH-CO-Distilled water	5.051	0.3988	0.929	1,250	0.0019	0.998	0.0679	10.25	0.0234	0.9736	Langmuir
RH-UMO-Raw water	7.003	0.3477	0.952	1,667	0.0033	0.999	0.0420	9.09	0.0595	0.9743	Langmuir
RH-CO-Raw water	5.981	0.3635	0.960	1,429	0.0022	0.999	0.0596	10.33	0.0373	0.9782	Langmuir
SD-UMO-Distilled water	5.153	0.33	0.826	769	0.0002	0.994	0.3399	18.39	0.0345	0.8857	Langmuir
SD-CO-Distilled water	4.227	0.3656	0.857	666	0.0002	0.998	0.3534	19.54	0.0217	0.9459	Langmuir
SD-UMO-Raw water	4.789	0.3855	0.843	1,000	0.0021	0.997	0.0627	12.86	0.0240	0.9149	Langmuir
SD-CO-Raw water	5.152	0.3404	0.916	833	0.0019	0.999	0.0685	16.38	0.0293	0.9883	Langmuir
SCB-UMO-Distilled water	4.334	0.42	0.878	1,111	0.0016	0.996	0.0777	11.30	0.0175	0.9522	Langmuir
SCB-CO-Distilled water	4.736	0.3727	0.931	909	0.0017	0.996	0.0760	14.18	0.0215	0.9664	Langmuir
SCB-UMO-Raw water	5.319	0.3771	0.847	1,111	0.0025	0.998	0.0537	11.39	0.0292	0.9367	Langmuir
SCB CO-Raw water	4.569	0.401	0.925	1,111	0.0016	0.999	0.0805	12.00	0.0193	0.9783	Langmuir
AC-UMO-Distilled water	7.039	0.363	0.954	2,000	0.0032	0.997	0.0433	8.06	0.0605	0.9479	Langmuir
AC-CO-Distilled water	6.117	0.3936	0.945	1,667	0.0024	0.991	0.0551	7.81	0.0374	0.9324	Langmuir
AC-UMO-Raw water	7.910	0.3543	0.867	2,000	0.0060	1.000	0.0240	7.32	0.0909	0.9434	Langmuir
AC-CO-Raw water	6.489	0.3891	0.973	2,000	0.0024	0.997	0.0547	7.49	0.0458	0.9677	Langmuir

Table 6
List of equations used in the adsorption kinetic modelling

Adsorption kinetic models	Linear equation	Non-linear equation
Pseudo-first-order model	$\log(q_e - q_t) = \log q_e - \frac{K_1}{2.303}t$	$\frac{dq_t}{dt} = K_1(q_e - q_t)^2$
Pseudo-second-order model	$\frac{t}{q_t} = \frac{1}{K_2 q_e^2} + \frac{1}{q_e}t$	$\frac{dq_t}{dt} = K_2(q_e - q_t)^2$
Intraparticle diffusion model	–	$q_t = K_i t^{1/2}$

RH, SD, SCB, and AC and the slope of each line gave the value of K_i. The kinetic model parameters and correlation coefficients (R^2) for the adsorption of UMO and CO for RH, SD, SCB and AC for distilled water and raw seawater are summarized in Table 7. By applying the pseudo-first-order kinetics model, the values of K_1 (1/min) were found to range from 0.0157 to 0.5 while the pseudo-second-order kinetics model gave values for K_2 that ranges from 0.000075 to 0.00167 min^{-1}. The values of the constant K_i in the intraparticle diffusion kinetics model ranged from 24.42 to 53.65. According to the correlation coefficient (R^2 values) obtained by plotting each model using the experimental data, it was found that the results are in agreement with the pseudo-second-order kinetics model than the other examined kinetics models. The results obtained in the current study exhibited similar trends to the results obtained by Soliman et al. [44] (magnetic wood sawdust), [48] (nano-silica and nano-zeolite from barley grass straw), [45] (activated charcoal from sawdust), [13] (natural and powdered corncob), [43] (algal biomass), [11] (corncob), [31] (modified rice husk), which obey the pseudo-second-order kinetics model.

5. Adsorption thermodynamics

It is worth mentioning that all the experiments were conducted at a fixed temperature of 25°C and the effect of temperature was not investigated in the current study. Thus, it is not possible to obtain all the thermodynamics parameters, that is, change in enthalpy ΔH and change in entropy ΔS. the only parameter that can be obtained is the change in Gibbs free energy, which can give an indication whether the oil sorption is spontaneous or not. The Gibbs free energy change (ΔG) can be calculated using Eqs. (3) and (4) as reported by Bonilla-Petriciolet et al. [49]:

$$\Delta G = -RT\ln K \quad (3)$$

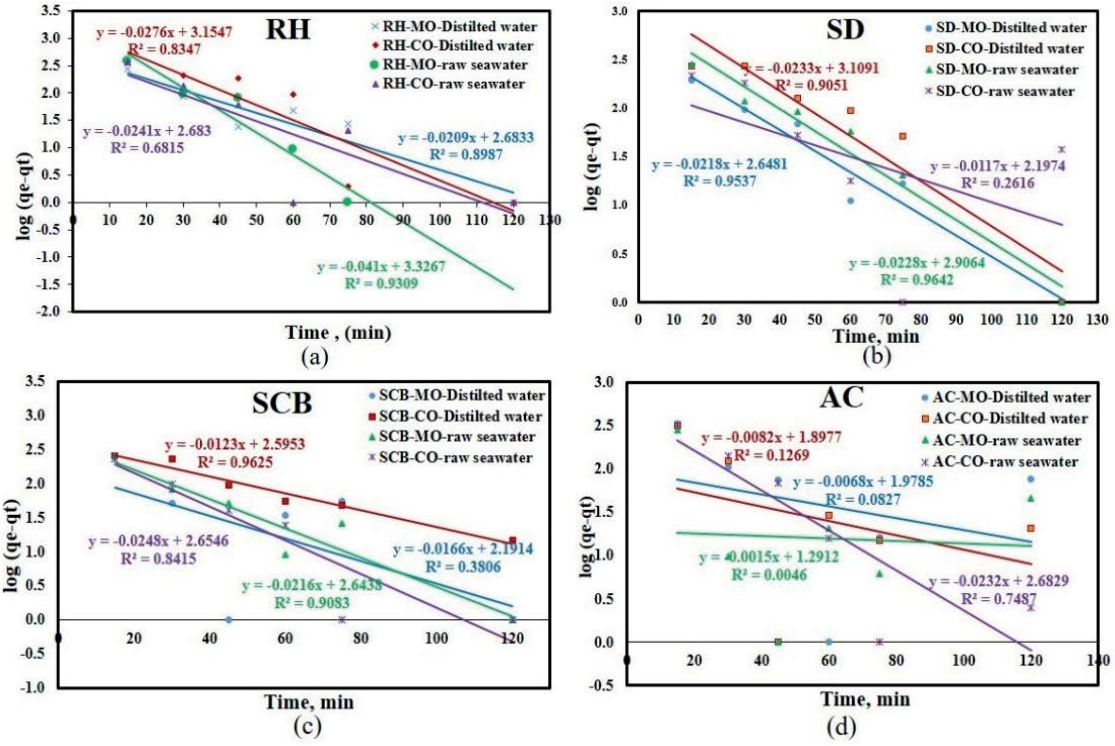

Fig. 16. Pseudo-first-order for rice husk, sawdust, sugarcane bagasse and activated carbon for adsorbed used motor oil and crude oil for distilled water and raw seawater at different oil concentrations.

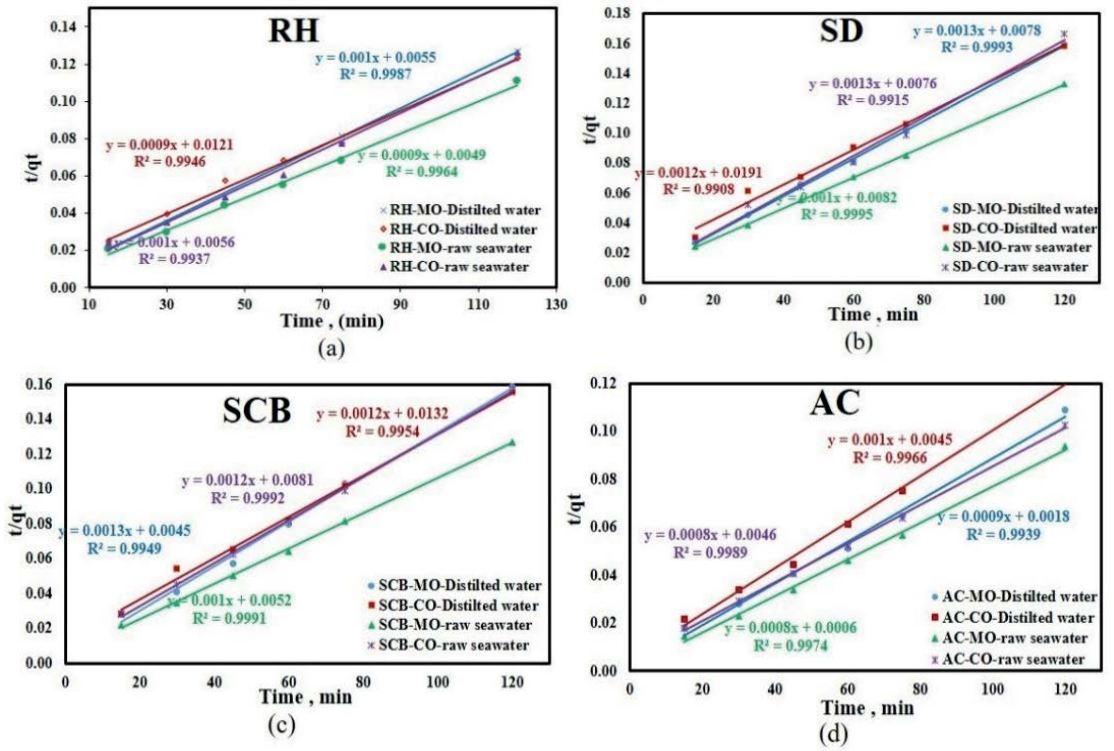

Fig. 17. Pseudo-second-order for rice husk, sawdust, sugarcane bagasse and activated carbon for adsorbed used motor oil and crude oil for distilled water and raw seawater at different oil concentrations.

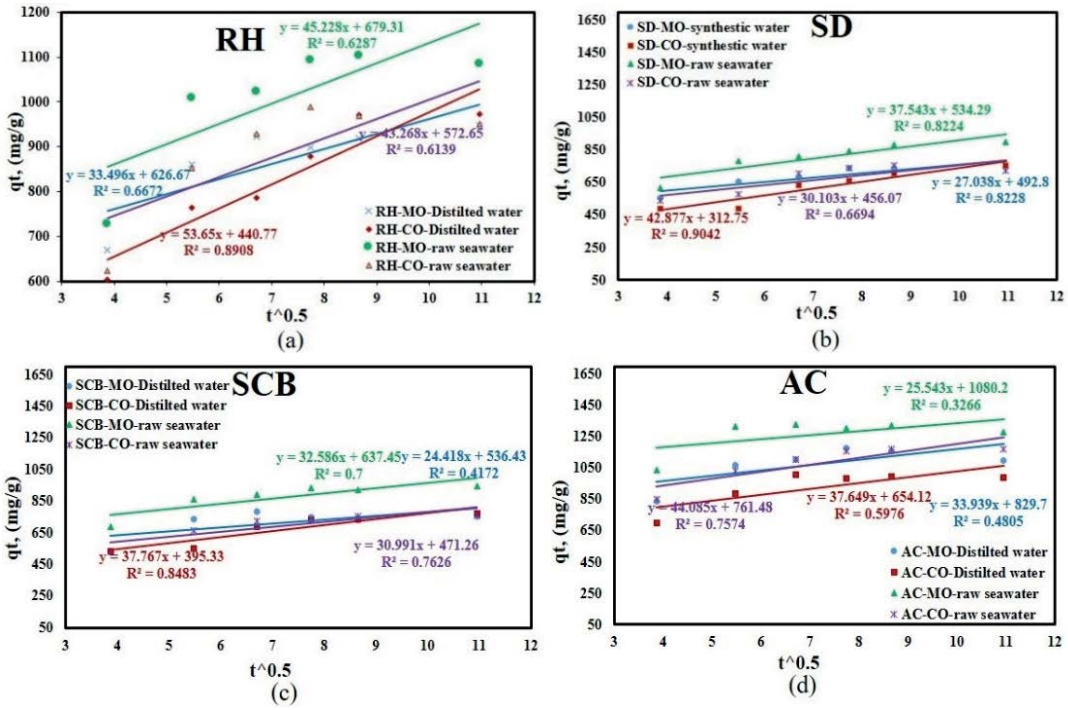

Fig. 18. Intraparticle diffusion model for rice husk, sawdust, sugarcane bagasse and activated carbon for adsorbed used motor oil and crude oil for distilled water and raw seawater at different oil concentrations.

Table 7
Pseudo-first-order, pseudo-second-order, and intraparticle diffusion kinetics model parameters and correlation coefficients for UMO and CO onto RH, SD, SCB and AC

Adsorbent type	Pseudo-first-order			Pseudo-second-order			Intraparticle diffusion		Favourable adsorption
	q_e (mg/g)	K_1 (1/min)	R^2	q_e (mg/g)	K_2 (g/mg·min)	R^2	K_i (mg/g·min$^{0.5}$)	R^2	
RH-UMO-Distilled water	482.28	0.0481	0.899	1,000	0.000182	0.999	33.50	0.667	Pseudo-second-order
RH-CO-Distilled water	1,427.9	0.0636	0.833	1,111	0.000067	0.995	53.65	0.891	Pseudo-second-order
RH-UMO-Raw seawater	2,121.7	0.0944	0.931	1,111	0.000165	0.996	45.23	0.629	Pseudo-second-order
RH-CO-Raw seawater	481.95	0.0555	0.682	1,000	0.000179	0.994	43.27	0.614	Pseudo-second-order
SD-UMO-Distilled water	444.73	0.5021	0.954	769.23	0.000217	0.999	27.04	0.823	Pseudo-second-order
SD-CO-Distilled water	1,285.5	0.0537	0.905	833.33	0.000075	0.991	42.88	0.904	Pseudo-second-order
SD-UMO-Raw seawater	806.12	0.0525	0.964	1,000	0.000122	0.999	37.54	0.822	Pseudo-second-order
SD-CO-Raw seawater	157.54	0.0269	0.262	769.23	0.000222	0.992	30.10	0.669	Pseudo-second-order
SCB-UMO-Distilled water	155.38	0.0382	0.381	769.23	0.000376	0.995	24.42	0.417	Pseudo-second-order
SCB-CO-Distilled water	343.16	0.0074	0.464	833.33	0.000109	0.995	37.77	0.848	Pseudo-second-order
SCB-UMO-Raw seawater	440.35	0.0497	0.908	1,000	0.000192	0.999	32.59	0.700	Pseudo-second-order
SCB CO-Raw seawater	451.44	0.0571	0.842	833.33	0.000178	0.999	30.99	0.763	Pseudo-second-order
AC-UMO-Distilled water	95.17	0.0157	0.083	1,111	0.000450	0.994	33.94	0.481	Pseudo-second-order
AC-CO-Distilled water	79.01	0.0189	0.127	1,000	0.000222	0.997	37.65	0.598	Pseudo-second-order
AC-UMO-Raw seawater	19.55	0.0035	0.005	1,250	0.001067	0.997	25.54	0.327	Pseudo-second-order
AC-CO-Raw seawater	481.84	0.0534	0.749	1,250	0.000139	0.999	44.09	0.757	Pseudo-second-order

$$K = \frac{\frac{q_e}{q_m}}{\left(1-\frac{q_e}{q_m}\right)\frac{C_e}{C_0}} \quad (4)$$

where T, R, q_e, q_m, C_o and C_e are the absolute temperature (K), gas constant (8.314 J/mol·K), equilibrium oil sorption capacity (mg/g), maximum oil sorption capacity (mg/g), initial oil concentration (mg/L) and equilibrium oil

concentration (mg/L), respectively. As mentioned above, the experiments were conducted at 25°C. The values of the thermodynamic parameter, Gibbs free energy (ΔG), are shown in Table 8. The values of ΔG are summarized in Table 8 and all the values are negative for all adsorbent in UMO and CO indicating that the adsorption process is spontaneous.

6. Comparison study

Table 9 summarizes the adsorption capacity and the experimental parameters for RH, SD, SCB and AC reported by other researchers for the sake of comparison with the results obtained in the current study. The comparison demonstrates that the oil adsorption capacity measured in the present study exhibits reasonable agreement with the values reported by other researchers. The differences may be attributed to the difference in experimental conditions and type of oil and water (raw seawater vs. distilled or synthetic seawater). In addition, it should be taken in consideration the characterization of adsorbent such as surface area, particle size … etc. as well as, the properties of oil, contaminated water, and environmental factors such as pH and temperature. Generally, different condition can affect

Table 8
Value of ΔG of RH, SD, SCB, and AC

Adsorbent type	*K*	ΔG° (kJ/mol)
RH-CO-Distilled water	15.699	–6.822
RH-CO-Distilled water	15.078	–6.722
RH-UMO-Raw water	20.737	–7.512
RH-CO-Raw water	16.280	–6.912
SD-UMO-Distilled water	46.283	–9.501
SD-CO-Distilled water	19.102	–7.308
SD-UMO-Raw water	33.944	–8.733
SD-CO-Raw water	17.017	–7.022
SCB-UMO-Distilled water	16.886	–7.003
SCB-CO-Distilled water	11.385	–6.026
SCB-UMO-Raw water	35.915	–8.873
SCB CO-Raw water	12.405	–6.239
AC-UMO-Distilled water	17.931	–7.152
AC-CO-Distilled water	13.203	–6.393
AC-UMO-Raw water	70.031	–10.527
AC-CO-Raw water	16.609	–6.962

Table 9
Adsorption capacity of RH, SD, SCB, and AC from other studies

Adsorbent type	Oil type	Water type	Process condition			Adsorption capacity, (mg/g)	References
			Oil concentration	Adsorbent dose	Contact time		
Raw SCB	Diesel oil	Artificial seawater	20 g/L	2 g/L	40 min	2,500	[16]
	Paraffin oil					2,700	
	Gasoline					2,300	
	Vegetable oil					2,600	
Raw SD	Diesel motor	Distilled water	50 mL	1 g	60 min	4,190	[36]
Raw SD	Used oils	Distilled water				4,280	
PAC	Emulsified oil	Produced water	1.613 g/L	0.5 g	120 min	468	[50]
Raw RH	Engine oil	Tap water	10 g/L	10 g/L	5 min	1,250	[31]
AC	CO	Distilled water	0.035 g/L	2 g	60 min	2,820	[37]
Raw RH	UMO	Distilled water	10 g/L	6 g/L	30 min	1,420	This study
Raw RH	UMO	Raw seawater				1,667	This study
Raw RH	CO	Distilled water				1,250	This study
Raw RH	CO	Raw seawater				1,429	This study
Raw SD	UMO	Distilled water				0769	This study
Raw SD	UMO	Raw seawater				1,000	This study
Raw SD	CO	Distilled water				666	This study
Raw SD	CO	Raw seawater				833	This study
Raw SCB	UMO	Distilled water				1,111	This study
Raw SCB	UMO	Raw seawater				1,111	This study
Raw SCB	CO	Distilled water				909	This study
Raw SCB	CO	Raw seawater				1,111	This study
Commercial AC	UMO	Distilled water				2,000	This study
Commercial AC	UMO	Raw seawater				2,000	This study
Commercial AC	CO	Distilled water				1,667	This study
Commercial AC	CO	Raw seawater				2,000	This study

the performance of adsorbents and oil adsorption capacity. It is not fair to conduct a comparison between the different adsorbents unless the experimental conditions are nearly the same.

7. Conclusions

The current study investigated the possibility of using agricultural waste-based adsorbents as a viable option for oil removal (CO and UMO) from seawater in the pre-treatment system of RO desalination plants. The investigated adsorbents included RH, SD, and SCB as well as AC. FTIR, SEM, and BET analysis was conducted to analyse the adsorbents surface. The following points can be withdrawn from the current study:

- RH achieved adsorption capacity which were about 30% lower than the values obtained with the tested commercial activated carbon. Thus, RH, as a low-cost adsorbent, can be used as a viable option to reduce the cost if we consider the production cost of the AC.
- The oil sorption removal decreases with increasing the initial oil concentration while it increases with increasing the adsorbent dose.
- The oil sorption removal and adsorption capacity increases with increasing the contact time and reaches the equilibrium state after 30 min for all cases except for CO in distilled water where it needed 45 min to reach the equilibrium and high sorption removal.
- The largest difference in oil sorption removal between raw and modified adsorbent in the current study is 26%. This indicates that the chemical treatment adopted in the present study has a small effect.
- The experimental adsorption data were described well by the Langmuir isotherm model while the adsorption kinetics were described by the pseudo-second-order model.
- The adsorption capacity depends strongly on the type of water (distilled vs. raw sweater) for some adsorbents (SCB and SD) while the effect of water type was weak for some other adsorbents (AC and RH). Thus, care should be taken when distilled water is used to stimulate the raw seawater.
- The oil sorption removal in synthetic saline water is nearly similar to that achieved in raw seawater where the difference between the two types of water was in the 2%–7%.
- Testing the effect of other metals ions on the oil adsorption indicated that the oil removal occurs at a faster rate compared to the metals ions. Therefore, the effect of other dissolved ions on oil removal can be neglected.

Acknowledgments

The Environmental Engineering Department, Zagazig University for providing supporting services and useful advice during the experimental stage of this work.

Symbols

C_e — Equilibrium concentration of oil, mg/L
ΔG — Change in Gibbs free energy, J/mol
q_e — Adsorption capacity at equilibrium concentration of oil, mg/g
q_{max} — Maximum adsorption capacities, mg/g
Q_0 — Maximum adsorption capacity, mg/g
n — Intensity of oil sorption
K_T — Equilibrium-binding constant corresponding to the maximum binding energy, L/g
R — Universal gas constant (J/mol·K) = 8.314
T — Temperature, K
b — Constant of Langmuir model, L/mg
K_f — Constant of Freundlich model, g/mg
B_T — Constant of Temkin model, L/g
q_t — Amount of oil adsorbed at any time t, min
K_1 — Constant of pseudo-first-order, 1/min
K_2 — Constant of pseudo-second-order, g/mg·min
K_i — Constant of intraparticle diffusion models, mg/g·min$^{0.5}$

References

[1] R.G. Abd Ellah, Water resources in Egypt and their challenges, Lake Nasser case study, Egypt. J. Aquat. Res., 46 (2020) 1–12.
[2] D. Janowitz, S. Groche, S. Yuce, T. Melin, T. Wintgens, Can large-scale offshore membrane desalination cost-effectively and ecologically address water scarcity in the middle east?, Membranes (Basel), 12 (2022) 323, doi: 10.3390/membranes12030323.
[3] S. Jiang, Y. Li, B.P. Ladewig, A review of reverse osmosis membrane fouling and control strategies, Sci. Total Environ., 595 (2017) 567–583.
[4] N. AlSawaftah, W. Abuwatfa, N. Darwish, G. Husseini, A comprehensive review on membrane fouling: mathematical modelling, prediction, diagnosis, and mitigation, Water, 13 (2021) 1327, doi: 10.3390/w13091327.
[5] M. Jafari, M. Vanoppen, J.M.C. van Agtmaal, E.R. Cornelissen, J.S. Vrouwenvelder, A. Verliefde, M.C.M. van Loosdrecht, C. Picioreanu, Cost of fouling in full-scale reverse osmosis and nanofiltration installations in the Netherlands, Desalination, 500 (2021) 114865, doi: 10.1016/j.desal.2020.114865.
[6] M. Qasim, M. Badrelzaman, N.N. Darwish, N.A. Darwish, N. Hilal, Reverse osmosis desalination: a state-of-the-art review. Desalination, 459 (2019) 59–104.
[7] S.G. Yiantsios, D. Sioutopoulos, A.J. Karabelas, Colloidal fouling of RO membranes: an overview of key issues and efforts to develop improved prediction techniques, Desalination, 183 (2005) 257–272.
[8] H. Sarkheil, J. Tavakoli, Oil-polluted water treatment using nano size bagasse optimized isotherm study, Eur. Online J. Nat. Social Sci., 4 (2015) 392–400.
[9] W. Jian, A. Kitanaka, W. Nishijima, A.U. Baes, M. Okada, Removal of oil pollutants in seawater as pretreatment of reverse osmosis desalination process, Water Res., 33 (1999) 1857– 1863.
[10] R. Asadpour, N.B. Sapari, M.H. Isa, S. Kakooei, K.U. Orji, Acetylation of corn silk and its application for oil sorption, Fibers Polym., 16 (2015) 1830–1835.
[11] J. Zhen, L. Hai, C. Yue-fang, D. Ying-bo, M. Imran, Corncob modified by lauric acid and ethanediol for emulsified oil adsorption, J. Cent. South Univ., 22 (2015) 2096−2105.
[12] D. Peng, L. Nie, F. Ouyang, L. Zheng, Research on green remediation technology of oil spill by biosorbent, IOP Conf. Ser.: Earth Environ. Sci., 171 (2018) 012044, doi: 10.1088/1755-1315/171/1/012044.
[13] H.-J. Choi, Agricultural bio-waste for adsorptive removal of crude oil in aqueous solution, J. Mater. Cycles Waste Manage., 21 (2019) 356–364.
[14] N.A. Abdelwahab, N. Shukry, S.F. El-kalyoubi, Preparation and characterization of polymer coated partially esterified sugarcane bagasse for separation of oil from seawater, Environ. Technol., 38 (2016) 1905–1914.

[15] N.A. Abdelwahab, N. Shukry, S.F. El-kalyoubi, Separation of emulsified oil from wastewater using polystyrene and surfactant modified sugarcane bagasse wastes blend, Clean Technol. Environ. Policy, 23 (2021) 235–249.
[16] O. Abdelwahab, S.M. Nasr, W.M. Thabet, Palm fibers and modified palm fibers adsorbents for different oils, Alexandria Eng. J., 56 (2017) 749–755.
[17] G. Alaa El-Din, A.A. Amer, G. Malsh, M. Hussein, Study on the use of banana peels for oil spill Removal, Alexandria Eng. J., 57 (2018) 2061–2068.
[18] M.A. Mahmoud, Oil spill cleanup by raw flax fiber: modification effect, sorption isotherm, kinetics and thermodynamics, Arabian J. Chem., 13 (2020) 5553–5563.
[19] S.N.C.M. Hussein, N.H. Othman, A. Dollah, A.N.C. Abdul Rahim, N.S. Japperi, N.S.M.A. Ramakrishnan, Study of acid treated mixed sawdust as natural oil sorbent for oil spill, Mater. Today Proc., 19 (2019) 1382–1389.
[20] S. El-Shahway, M.M.A. Mahmoud, T.K. Udeigwe, Alterations in soil chemical properties induced by continuous rice cultivation: a study on the arid Nile delta soils of Egypt, Land Degrad. Dev., 27 (2016) 231–238.
[21] A. Michael, R.R. Moussa, Evaluating the effect of adding sugarcane bagasse to the fire clay brick's properties, Civ. Eng. Archit., 10 (2022) 71–78.
[22] S. Kumagai, Y. Noguchi, Y. Kurimoto, K. Takeda, Oil adsorbent produced by the carbonization of rice husks, Waste Manage., 27 (2007) 554–561.
[23] M.A. Mahmud, F.R. Anannya, Sugarcane bagasse – a source of cellulosic fiber for diverse applications, Heliyon, 7 (2021) e07771, doi: 10.1016/j.heliyon.2021.e07771.
[24] ASTM-F726-12, Standard Test Method for Sorbent Performance of Adsorbents, 2012.
[25] A. Bazargan, J. Tan, G. McKay, Standardization of oil sorbent performance testing, J. Test. Eval., 43 (2015), doi: 10.1520/JTE20140227.
[26] A.B.D. Nandiyanto, R. Oktiani, R. Ragadhita, How to read and interpret FTIR spectroscope of organic material, Indones. J. Sci. Technol., 4 (2019) 97–118.
[27] M. Bansal, U. Garg, D. Singh, V.K. Garg, Removal of Cr(VI) from aqueous solutions using pre-consumer processing agricultural waste: a case study of rice husk, J. Hazard. Mater., 162 (2009) 312–320.
[28] W.A.W.A.K. Ghani, A. Mohd, G. da Silva, R.T. Bachmann, Y.H. Taufiq-Yab, U. Rashid, A.H. Al-Muhtaseb, Biochar production from waste-rubber-wood sawdust and its potential use in C sequestration: chemical and physical characterization, Ind. Crops Prod., 44 (2013) 18–24.
[29] N.S. Abdul Hamid, N.A.C. Malek, H. Mokhtar, W.S. Mazlan, R.M. Tajuddin, Removal of oil and grease from wastewater using natural adsorbents, J. Teknologi (Sciences & Engineering), 78 (2016) 97–102.
[30] S. Ehsan, Y. Majid, E.A. Abtin, Comparison of adsorption properties of activated carbons with different crops residues as precursors for gold cyanide recovery: an Iranian gold industry guide, Iran. J. Chem. Chem. Eng., 39 (2020) 213–229.
[31] Z. Razavi, N. Mirghaffari, B. Rezaei, Adsorption of crude and engine oils from water using raw rice husk, Water Sci Technol., 69 (2014) 947–952.
[32] W.S. Ngah, M.A. Hanafiah, Biosorption of copper ions from dilute aqueous solution on base treated rubber (*Hevea brasiliensis*) leaves powder: kinetics, isotherm, and biosorption mechanism, J. Environ. Sci., 20 (2008) 1168–1176.
[33] U.A. Abel, G.R. Habor, O.I. Oseribho, Adsorption studies of oil spill clean-up using coconut coir activated carbon (CCAC), Am. J. Chem. Eng., 8 (2020) 36–47.
[34] T.-T. Lim, X. Huang, Evaluation of kapok (*Ceiba pentandra* (L.) Gaertn.) as a natural hollow hydrophobic–oleophilic fibrous sorbent for oil spill cleanup, Chemosphere, 66 (2007) 955–963.
[35] A. Bayat, S.F. Aghamiri, A. Moheb, Oil sorption by synthesized exfoliated graphite (EG), Iran. J. Chem. Eng., 5 (2008) 51–64.
[36] B. Nechchadi, H. Ghazzaf, N. Mazoir, E.K. Lhadi, M. El. Krati, S. Tahiri, Oil removal from water through the sorption on natural agrowaste materials, J. Environ. Eng., 146 (2020), doi: 10.1061/(ASCE)EE.1943-7870.0001802.
[37] A. Olufemi, F. Otolorin, Comparative adsorption of crude oil using mango (*Mangnifera indica*) shell and mango shell activated carbon, Environ. Eng. Res., 22 (2017) 384–392.
[38] M. Bjelopavlic, G. Newcombe, R. Hayes, Adsorption of NOM onto activated carbon: effect of surface charge, ionic strength, and pore volume distribution, J. Colloid Interface Sci., 210 (1999) 271–280.
[39] Y.-S. Yun, D. Park, S.R. Lim, J.M. Park, Kinetic analysis and mathematical modeling of Cr (VI) removal in a differential reactor packed with Ecklonia biomass, J. Microbiol. Biotechnol., 16 (2006) 1720–1727.
[40] C. Aharoni, M. Ungarish, Kinetics of activated chemisorption. Part 2.—theoretical models, J. Chem. Soc., Faraday Trans. 1 F, 1 (1977) 456–464.
[41] M. Temkin, V. Pyzhev, Kinetics of the synthesis of ammonia on promoted iron catalysts, Acta Physiochim. USSR, 12 (1940) 217–222.
[42] N.E. Thompson, G.C. Emmanuel, K.J. Adagadzu, N.B. Yusuf, Sorption studies of crude oil on acetylated rice husks, Arch. Appl. Sci. Res., 2 (2010) 142–151.
[43] H. Boleydei, N. Mirghaffari, O. Farhadian, Comparative study on adsorption of crude oil and spent engine oil from seawater and freshwater using algal biomass, Environ. Sci. Pollut. Res., 25 (2018) 21024–21035.
[44] E.M. Soliman, A. Salwa, A. Aliaa, A. Fadl, Adsorptive removal of oil spill from sea water surface using magnetic wood sawdust as a novel nano-composite synthesized via microwave approach, J. Environ. Health Sci. Eng., 18 (2020) 79–90.
[45] K. Rajak, S. Kumar, N.V. Thombre, A. Mandal, Synthesis of activated charcoal from sawdust and characterization for adsorptive separation of oil from oil-in water emulsion, Chem. Eng. Commun., 205 (2018) 1–17.
[46] S. Largergren, About the theory of so-called adsorption of soluble substances, Kungliga Svenska Vetenskapsakademiens, Handlingar, 24 (1898) 1–39.
[47] Y.S. Ho, G. McKay, Pseudo-second-order model for sorption processes, Process Biochem., 34 (1999) 451–465.
[48] E. Akhayere, D. Kavaz, Nano-silica and nano-zeolite synthesized from barley grass straw for effective removal of gasoline from aqueous solution: a comparative study, Chem. Eng. Commun., 208 (2021) 1419–1435.
[49] A. Bonilla-Petriciolet, D.L. Mendoza-Castillo, H.E. Reynel-Avila, Adsorption Processes for Water Treatment and Purification, Springer International Publishing, Springer Cham, 2017.
[50] K. Okiel, M. El-Sayed, M.Y. El-Kady, Treatment of oil–water emulsions by adsorption onto activated carbon, bentonite and deposited carbon, Egypt. J. Pet., 20 (2011) 9–15.